



Universiteit  
Leiden  
The Netherlands

## Immunosuppression in breast cancer: a closer look at regulatory T cells

Kos, K.

### Citation

Kos, K. (2023, January 11). *Immunosuppression in breast cancer: a closer look at regulatory T cells*. Retrieved from <https://hdl.handle.net/1887/3505617>

Version: Publisher's Version

License: [Licence agreement concerning inclusion of doctoral thesis in the Institutional Repository of the University of Leiden](#)

Downloaded from: <https://hdl.handle.net/1887/3505617>

**Note:** To cite this publication please use the final published version (if applicable).



# 4

## Tumor-educated T<sub>regs</sub> drive organ-specific metastasis in breast cancer by impairing NK cells in the lymph node niche

Kevin Kos<sup>1,2</sup>, Muhammad A. Aslam<sup>1,3,11</sup>, Rieneke van de Ven<sup>4,9,11</sup>, Max D. Wellenstein<sup>1,2,10</sup>, Wietske Pieters<sup>1</sup>, Antoinette van Weverwijk<sup>1,2</sup>, Danique E.M. Duits<sup>1,2</sup>, Kim van Pul<sup>4</sup>, Cheei-Sing Hau<sup>1,2</sup>, Kim Vrijland<sup>1,2</sup>, Daphne Kaldenbach<sup>1,2</sup>, Elisabeth A.M. Raeven<sup>1,2</sup>, Sergio A. Quezada<sup>5</sup>, Rudi Beyaert<sup>6,7</sup>, Heinz Jacobs<sup>1</sup>, Tanja D. de Groot<sup>4</sup>, Karin E. de Visser<sup>1,2,8,12</sup>

### Affiliations

<sup>1</sup> Division of Tumor Biology & Immunology, Netherlands Cancer Institute; 1066 CX Amsterdam, The Netherlands

<sup>2</sup> Oncode Institute, Utrecht; The Netherlands

<sup>3</sup> Institute of Molecular Biology and Biotechnology, Bahauddin Zakariya University; 60800 Multan, Pakistan

<sup>4</sup> Department of Medical Oncology, Amsterdam UMC, Vrije Universiteit Amsterdam, Cancer Center Amsterdam and Amsterdam Institute for Infection and Immunity; 1081 HV Amsterdam, The Netherlands

<sup>5</sup> Cancer Immunology Unit, University College London Cancer Institute; WC1E 6DD London, UK

<sup>6</sup> Center for Inflammation Research, Unit of Molecular Signal Transduction in Inflammation, VIB; 9052 Ghent, Belgium

<sup>7</sup> Department of Biomedical Molecular Biology, Ghent University; 9052 Ghent, Belgium

<sup>8</sup> Department of Immunology, Leiden University Medical Center; Leiden, The Netherlands.

<sup>9</sup> Current address: Department of Otolaryngology/Head-Neck Surgery, Amsterdam UMC, Vrije Universiteit Amsterdam, Cancer Center Amsterdam and Amsterdam Institute for Infection and Immunity; 1081 HV Amsterdam, The Netherlands

<sup>10</sup> Current address: Hubrecht Institute, Royal Netherlands Academy of Arts and Sciences (KNAW) and University Medical Center Utrecht; 3584 CT Utrecht, The Netherlands

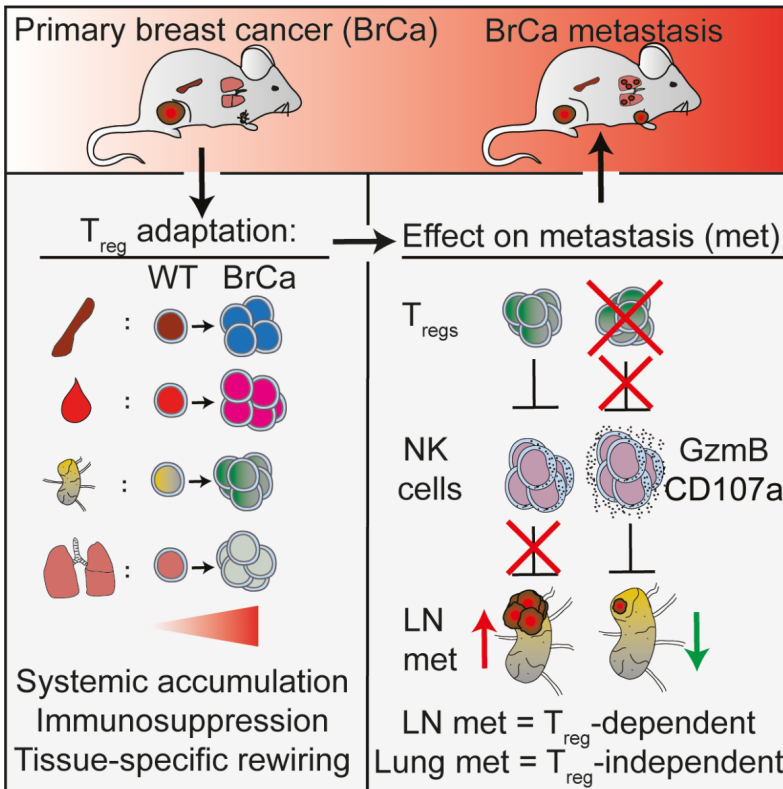
<sup>11</sup> These authors contributed equally

<sup>12</sup> Corresponding author: k.d.visser@nki.nl

**ABSTRACT**

Breast cancer is accompanied by systemic immunosuppression which facilitates metastasis formation, but how this shapes organotropism of metastasis is poorly understood. Here, we investigate the impact of mammary tumorigenesis on  $T_{regs}$  in distant organs and how this impacts multi-organ metastatic disease. Using a preclinical mouse mammary tumor model that recapitulates human metastatic breast cancer, we observe systemic accumulation of activated, highly immunosuppressive  $T_{regs}$  during primary tumor growth. Tumor-educated  $T_{regs}$  show tissue-specific transcriptional rewiring in response to mammary tumorigenesis. This has functional consequences for organotropism of metastasis, as  $T_{reg}$  depletion reduces metastasis to tumor-draining lymph nodes, but not to lungs. Mechanistically, we find that  $T_{regs}$  control NK cell activation in lymph nodes, thereby facilitating lymph node metastasis. In line, an increased  $T_{reg}$ /NK cell ratio is observed in sentinel lymph nodes of breast cancer patients compared to healthy controls. This study highlights that immune regulation of metastatic disease is highly organ dependent.

**Graphical Abstract**



## INTRODUCTION

The main cause of breast cancer-related mortality is metastatic disease. Over the past decades, breast cancer survival has improved through detection and intervention in early stages of breast cancer, but preventing and treating metastasis remains an unmet clinical need<sup>1</sup>. Disseminated cancer cells progress through a multistep cascade, which involves complex interactions between cancer- and host cells, including immune cells<sup>2</sup>. The immune system plays a dual role in metastasis formation. While properly activated cytotoxic immune cells are equipped to control metastasis, tumor-induced immunosuppressive immune cells exploit a diversity of mechanisms to promote metastasis<sup>3</sup>. Emerging data indicate that tissue tropism of metastasis may be influenced by the immune contexture in distant organs, suggesting an additional layer of complexity in metastasis formation<sup>4</sup>. However, how immunosuppressive mechanisms differ per metastatic site, and how this shapes tissue tropism of metastasis, is poorly understood.

An important cell type involved in immunosuppression in cancer is the CD4<sup>+</sup>FOXP3<sup>+</sup> regulatory T cell (T<sub>reg</sub>)<sup>5-7</sup>. In breast cancer, immunosuppressive T<sub>regs</sub> densely populate human tumors, and high levels of intratumoral T<sub>regs</sub> correlate with high tumor grade and poor survival<sup>6,8</sup>. Intriguingly, clinical data suggest that primary breast tumors impact T<sub>regs</sub> beyond the tumor micro-environment. T<sub>regs</sub> in peripheral blood have been reported to be increased in breast cancer patients<sup>9-12</sup>, and their responsiveness to cytokine stimulation is predictive of breast cancer relapse<sup>13</sup>. In addition, recent studies have shown that T<sub>regs</sub> accumulate in sentinel lymph nodes (LNs) of breast cancer patients, which correlates with cancer spread to these LNs<sup>14-18</sup>, suggesting a potential role for T<sub>regs</sub> in modulating metastasis to tumor-draining LNs.

Despite these intriguing clinical observations, and the attention that tumor-associated T<sub>regs</sub> have received in the context of breast cancer in recent years<sup>7,19</sup>, the lack of preclinical models that closely recapitulate human multi-organ metastatic disease has limited our understanding of the importance of T<sub>regs</sub> in cancer spread to different distant organs<sup>20</sup>. Preclinical studies performed with mouse models based on orthotopic inoculation of breast cancer cell lines have shown that ablation of T<sub>regs</sub> can attenuate primary tumor growth and subsequent metastasis formation to the lungs<sup>21-23</sup>. However, research on T<sub>regs</sub> in the context of cancer is mostly focused on their role in the micro-environment of primary tumors or metastases. The systemic impact of primary tumors on T<sub>regs</sub> in distant organs, and their functional significance for metastasis formation in different tissue contexts has remained largely unclear. Additionally, the role of T<sub>regs</sub> in hallmarks of metastatic disease such as systemic immunosuppression and the development of a pre-metastatic niche is understudied<sup>3</sup>, and therefore remains elusive.

Here we describe how mammary tumors systemically rewire  $T_{regs}$ , and how this impacts metastatic disease to different organs. To achieve this, we utilized models that allow for interrogation of tissue-specific metastasis, *i.e.* the transgenic *Keratin14 (K14)-cre;Cdh1<sup>F/F</sup>;Trp53<sup>F/F</sup>* (KEP) mouse model of invasive mammary tumorigenesis<sup>24</sup>, and the KEP-based mastectomy model for spontaneous multi-organ metastatic disease<sup>25</sup>. We observed systemic accumulation of activated, highly immunosuppressive  $T_{regs}$  during primary tumor growth. These  $T_{regs}$  showed striking tissue-specific transcriptional rewiring in response to mammary tumorigenesis, and elicited a tissue-specific effect on metastasis formation, as neoadjuvant depletion of  $T_{regs}$  reduced cancer spread to axillary (Ax.) LNs, but not to the lungs. Mechanistically, we demonstrate that  $T_{regs}$  promote LN metastasis formation through inhibition of NK cells in the lymph node niche. These findings add another mechanism to the emerging body of literature that immune regulation of metastatic disease is highly organ dependent, warranting a more personalized approach in the fight against metastatic disease.

## RESULTS

### Primary mammary tumors induce systemic expansion and activation of $T_{regs}$

To assess whether *de novo* mammary tumor formation exerts a systemic impact on  $T_{regs}$ , we examined the abundance, phenotype and activation status of  $T_{regs}$  in tumors, blood, and distant organs of the KEP mouse model, which spontaneously develops mammary tumors at 6-8 months of age resembling human invasive lobular carcinomas (ILC)<sup>24</sup>. We observed that mammary KEP tumors are highly infiltrated by FOXP3<sup>+</sup>CD4<sup>+</sup> T cells, as compared to healthy mammary glands of age-matched wild-type (WT) littermate controls (Fig. 1A, 1B). Interestingly, increased frequencies and absolute counts of  $T_{regs}$  were also observed in blood and in loco-regional or distant organs that are conducive to metastatic spread such as tumor draining LNs (TDLNs, axillary and inguinal, dependent on the location of the primary mammary tumor), spleen, lungs and non-draining LNs (NDLNs) of KEP mice bearing end-stage mammary tumors (225mm<sup>2</sup>) (Fig. 1A, C, S1A-B). Notably, we did not find a relative increase in CD4<sup>+</sup>FOXP3<sup>-</sup>, or CD8<sup>+</sup> T cells (with the exception of CD8<sup>+</sup> T cells in TDLNs) in tumor-bearing KEP mice (Fig. 1D, S1C-D). An increase in absolute cell counts was also observed for CD4<sup>+</sup>FOXP3<sup>-</sup> and CD8<sup>+</sup> T cells in LNs and tumors (Fig. S1E-G), due to expansion of these tissue compartments in KEP mice versus WT controls. However, comparing the ratio of FOXP3<sup>+</sup>/CD8<sup>+</sup> and FOXP3<sup>+</sup>/FOXP3<sup>-</sup> cells in different tissues of tumor-bearing KEP mice and WT controls (Fig. S1H-I) confirmed that mammary tumorigenesis specifically and systemically expands  $T_{regs}$  amongst the adaptive immune cell compartment. We then assessed whether  $T_{reg}$  expansion is explained by their increased proliferation or survival in tumor-bearing KEP mice. Ki67 expression on  $T_{regs}$  in tumor-bearing KEP mice was found to be uniquely increased in LNs, compared to WT controls (Fig. S1J). Notably,

no difference was observed between TDLNs and NDLNs showing T<sub>reg</sub> proliferation is systemically increased in LNs of tumor-bearing KEP mice (Fig. S1K). Furthermore, KEP T<sub>regs</sub> showed increased viability when exposed to serum obtained from tumor-bearing KEP mice, as opposed to serum obtained from WT mice (Fig. S1L). Combined, these data suggest that LNs may be an important site for T<sub>reg</sub> proliferation in KEP mice, and that a soluble factor in KEP serum may contribute to increased T<sub>reg</sub> survival.

To investigate whether this systemic increase of T<sub>regs</sub> is consistently observed across pre-clinical mouse models of breast cancer, we analyzed T<sub>reg</sub> frequency in five different transgenic mouse models that represent different subsets of human breast cancers (Fig. 1E). Indeed, we found T<sub>regs</sub> to be significantly increased in the blood of tumor-bearing mice of all five models compared to WT controls, indicating systemic T<sub>reg</sub> expansion is a prevalent feature of mammary tumorigenesis.

Using high-dimensional flow cytometry, we observed that T<sub>regs</sub> both in- and outside of mammary tumors, have increased expression of surface proteins associated with T<sub>reg</sub> activation and suppressor function including CTLA4, ICOS, and CD103 in KEP tumor-bearing mice compared to WT controls, showing that these cells undergo a profound phenotypic change during mammary tumor progression (Fig. 1F, S1M-N). To address whether the enhanced activation state of KEP T<sub>regs</sub> impacts their functionality throughout the tumor-bearing host, we FACS sorted T<sub>regs</sub> from TDLNs, spleen and tumors from KEP mice and WT controls to assess their suppressive activity on the proliferation of CD4<sup>+</sup> and CD8<sup>+</sup> T cells *in vitro*. Regardless of the tissue of origin, T<sub>regs</sub> from tumor-bearing mice were significantly more potent in suppressing T cell proliferation compared to T<sub>regs</sub> isolated from WT mice (Fig. 1G-J), indicating that tumor-educated T<sub>regs</sub> have enhanced immunosuppressive potential, both intratumorally, as well as in TDLNs and spleen.

We next determined the dynamics of T<sub>reg</sub> accumulation and education by following T<sub>reg</sub> frequency and phenotype in aging KEP mice (from 2 to 8 months of age). Around 3 months of age, most KEP mice display microscopic neoplastic lesions in their mammary glands which over time progress into palpable mammary tumors, with a median latency of 6-8 months<sup>24</sup>. T<sub>reg</sub> frequency in blood gradually increased during neoplastic progression in KEP mice, and was significantly increased in KEP mice of 7 months and older prior to the onset of palpable mammary tumors, as compared to age-matched controls (Fig. 1K). Further analysis of these T<sub>regs</sub> showed that the impact of mammary tumorigenesis on T<sub>reg</sub> phenotype showed different kinetics per protein. Whereas the expression of CTLA4 increased prior to the development of palpable tumors, the expression of ICOS and CD103 was exclusively increased in tumor-bearing KEP mice (Fig. 1L, S1O-P). Together, these data demonstrate that primary mammary tumorigenesis engages T<sub>regs</sub> beyond the tumor microenvironment, leading to their systemic expansion and activation.

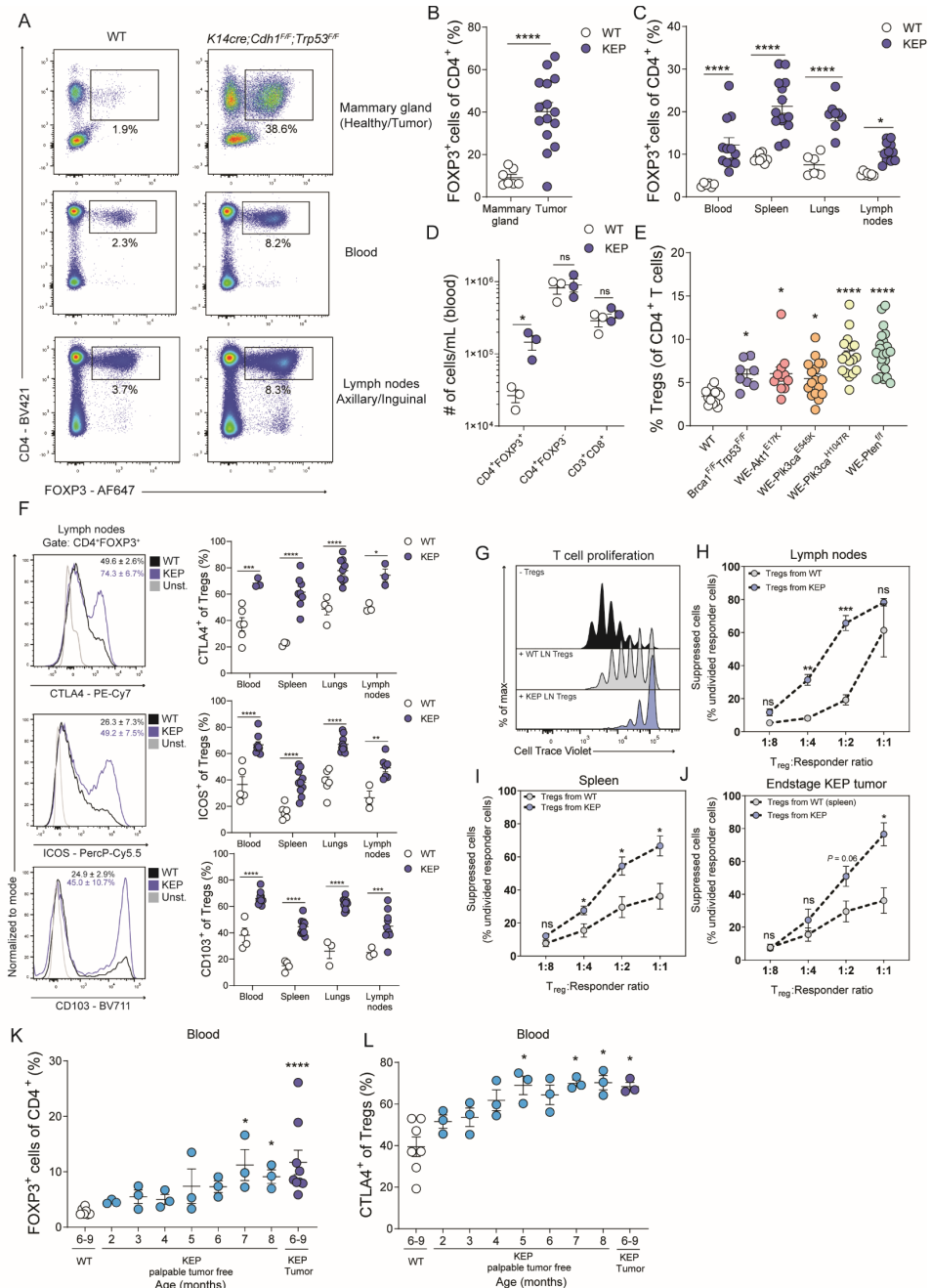


**FIGURE 1. Primary mammary tumors induce systemic expansion and activation of CD4<sup>+</sup>FOXP3<sup>+</sup> T cells.**

**A.** Representative dot plots depicting the CD4<sup>+</sup>FOXP3<sup>+</sup> T<sub>reg</sub> population (%) gated on live, CD45<sup>+</sup>CD3<sup>+</sup> cells in indicated tissues of *K14cre;Cdh1<sup>fl/fl</sup>;Trp53<sup>fl/fl</sup>* (KEP) mice bearing (225mm<sup>2</sup>) mammary tumors versus WT controls. **B-C.** Frequencies of FOXP3<sup>+</sup> cells of CD4<sup>+</sup> T cells in indicated tissues of KEP



mice bearing mammary tumors (225mm<sup>2</sup>) versus WT controls (n=6-15 mice/group) as determined by flow cytometry. **D.** Quantification of absolute cell counts of indicated adaptive immune cell populations per mL of blood of KEP mice bearing mammary tumors (225mm<sup>2</sup>) versus WT controls (n=3 mice/group). **E.** Frequencies of FOXP3<sup>+</sup> cells of CD4<sup>+</sup> T cells in blood of mice bearing end-stage tumors of indicated transgenic mouse models for mammary tumorigenesis compared to age-matched WT mice (n=8-22 mice/group). **F.** Representative histograms depicting expression (left) and quantification (right) of CTLA4, ICOS and CD103 gated on CD4<sup>+</sup> FOXP3<sup>+</sup> T cells, in indicated tissues of KEP mice (blue) bearing (225mm<sup>2</sup>) tumors versus WT littermates (black) by flow cytometry (n=3-11 mice/group). **G.** Representative histogram plots of CTV expression in activated CD4/CD8 T cells alone (black) or upon co-culture with CD4<sup>+</sup>CD25<sup>+</sup> cells (grey and blue) obtained from indicated tissues at 1:2 T<sub>reg</sub>:responder ratio. **H-J.** Quantification of undivided responder cells (CD8<sup>+</sup> and CD4<sup>+</sup> T cells) based on CTV expression, upon co-culture with CD4<sup>+</sup>CD25<sup>+</sup> isolated from indicated tissues at various ratios (data pooled from 3-4 independent experiments, with 2 technical replicates per experiment). **K.** Frequencies of FOXP3<sup>+</sup> cells of CD4<sup>+</sup> T cells in blood of tumor-free, tumor-bearing (225mm<sup>2</sup>) KEP mice and WT controls. (n=3-9 mice/group). **L.** Frequencies of CTLA4<sup>+</sup> cells of FOXP3<sup>+</sup>CD4<sup>+</sup> T cells in blood of tumor-free, tumor-bearing (225mm<sup>2</sup>) KEP mice and WT controls (n=3-7 mice/group). Data in B-F, H-L show mean ± S.E.M. P-values determined by unpaired Student's t-test (B, D, H, I, J), One-way ANOVA with Dunnett's multiple comparison test (E), Two-way ANOVA with Sidak's multiple comparison test (C,F), and Kruskal-Wallis test with Dunn's multiple comparison test (K,L). Asterisks indicate statistically significant differences compared to WT. \* P < 0.05, \*\* P < 0.01, \*\*\* P < 0.001, \*\*\*\* P < 0.0001.

### Mammary tumors alter the transcriptome of T<sub>regs</sub> in tumors and distant organs

To delineate the impact of mammary tumor progression on T<sub>regs</sub> in distant organs, RNA sequencing was performed on T<sub>regs</sub> (CD4<sup>+</sup>CD25<sup>high</sup>) isolated from blood, TDLNs, lungs, spleens, healthy mammary glands, and mammary tumors (225mm<sup>2</sup>) from tumor-bearing KEP mice and WT controls (Fig. 2A). Importantly, CD4<sup>+</sup>CD25<sup>high</sup> cells isolated from these tissues showed high and equal FOXP3 expression (Fig. S2A). Principal Component Analysis (PCA) showed distinct clustering of T<sub>regs</sub>, based on their residence in either lymphoid tissue (spleen and LNs) and blood, or residence in peripheral tissue (lungs, tumor, mammary gland) (Fig. 2B). Furthermore, T<sub>regs</sub> residing in distant organs cluster together independent of tumor status, whereas the gene expression profiles of tumor- and mammary gland T<sub>regs</sub> appear very distinct. Indeed, differential gene expression analysis comparing intratumoral KEP T<sub>regs</sub> and mammary tissue-resident T<sub>regs</sub> revealed 3707 differentially expressed genes (Fig. 2C). Ingenuity Pathway Analysis (IPA) showed the significantly changed pathways between T<sub>regs</sub> from tumors and mammary glands to pertain to cell migration and extravasation (Fig. 2D), which is underscored by some of the most differentially expressed genes, including *Mmp10*, *Mmp13* and *Ccr8* (data file S1). We confirmed by gene set enrichment analysis (GSEA) that intratumoral KEP T<sub>regs</sub> are significantly enriched for a clinically relevant cross-species and cross-tumor model tumor-infiltrating T<sub>regs</sub> (TIT<sub>regs</sub>) signature<sup>26</sup> (Fig. 2E).

Next, we sought to explore how mammary tumorigenesis affects T<sub>regs</sub> in distant organs by comparing gene expression profiles of KEP versus WT T<sub>regs</sub> from matched tissues. This comparison identified differential gene regulation in T<sub>regs</sub> in all organs tested, indicating that mammary tumors induce systemic transcriptional changes in T<sub>regs</sub> (Fig. 2F). To further map

these differentially regulated genes and their occurrence across different tissues, we analyzed their distribution in KEP versus WT  $T_{regs}$  across tissues (Fig. 2G). Doing so, we identified a set of 31 core genes to be significantly different (27 upregulated, 3 downregulated, 1 bi-directional dependent on tissue) in KEP  $T_{regs}$  regardless of tissue residence, suggesting a certain level of convergent, tissue-independent transcriptional rewiring in response to mammary tumorigenesis (Fig. 2H). Among those upregulated, we found genes encoding proteins important for T cell activation and the immunosuppressive features of  $T_{regs}$ , such as *Icos*, *Klrg1*, *Havcr2*, *Tigit* and *Tnfrsf9*. KEP  $T_{regs}$  were also found to have enhanced gene expression of *Gzmb*, which is known for its cytolytic function in NK and CD8<sup>+</sup> T cells, but has been shown to contribute to immunosuppression when expressed by  $T_{regs}$ <sup>27</sup>. Combined, these data suggest that mammary tumorigenesis enhances systemic immunosuppression through transcriptional rewiring of  $T_{regs}$  in distant organs.

We additionally identified *Il1rl1*, a gene encoding the IL-33 receptor ST2 to be systemically increased in KEP  $T_{regs}$  compared to WT  $T_{regs}$ , which was confirmed by FACS analysis (Fig. S2B-C). IL-33/ST2 signaling on  $T_{regs}$  has recently been described to induce a pro-tumorigenic phenotype in intratumoral  $T_{regs}$ <sup>28-30</sup> and has also been shown to drive expansion of  $T_{regs}$  *in vitro* and *in vivo*<sup>31</sup>. In KEP mice, IL-33 was found to be significantly increased in TDLNs compared to WT LNs, which was not observed in blood, tumor or lungs (Fig. S2D). Nevertheless, short-term neutralization of IL-33 in tumor-bearing KEP mice utilizing two independent approaches *i.e.* treatment of mice with anti-IL-33 or with an IL-33 antagonist (IL-33 Trap<sup>32</sup>) (Fig. S2E) did not alter systemic  $T_{reg}$  accumulation, proliferation, or phenotype (Fig. S2F-I), suggesting that in mice with established mammary tumors, the presence of the ST2<sup>+</sup>  $T_{reg}$  population is maintained independent of endogenous IL-33.

Taken together, these data demonstrate that mammary tumorigenesis induces systemic transcriptional rewiring of  $T_{regs}$ , sharing a core set of genes associated with  $T_{reg}$  function and activation.

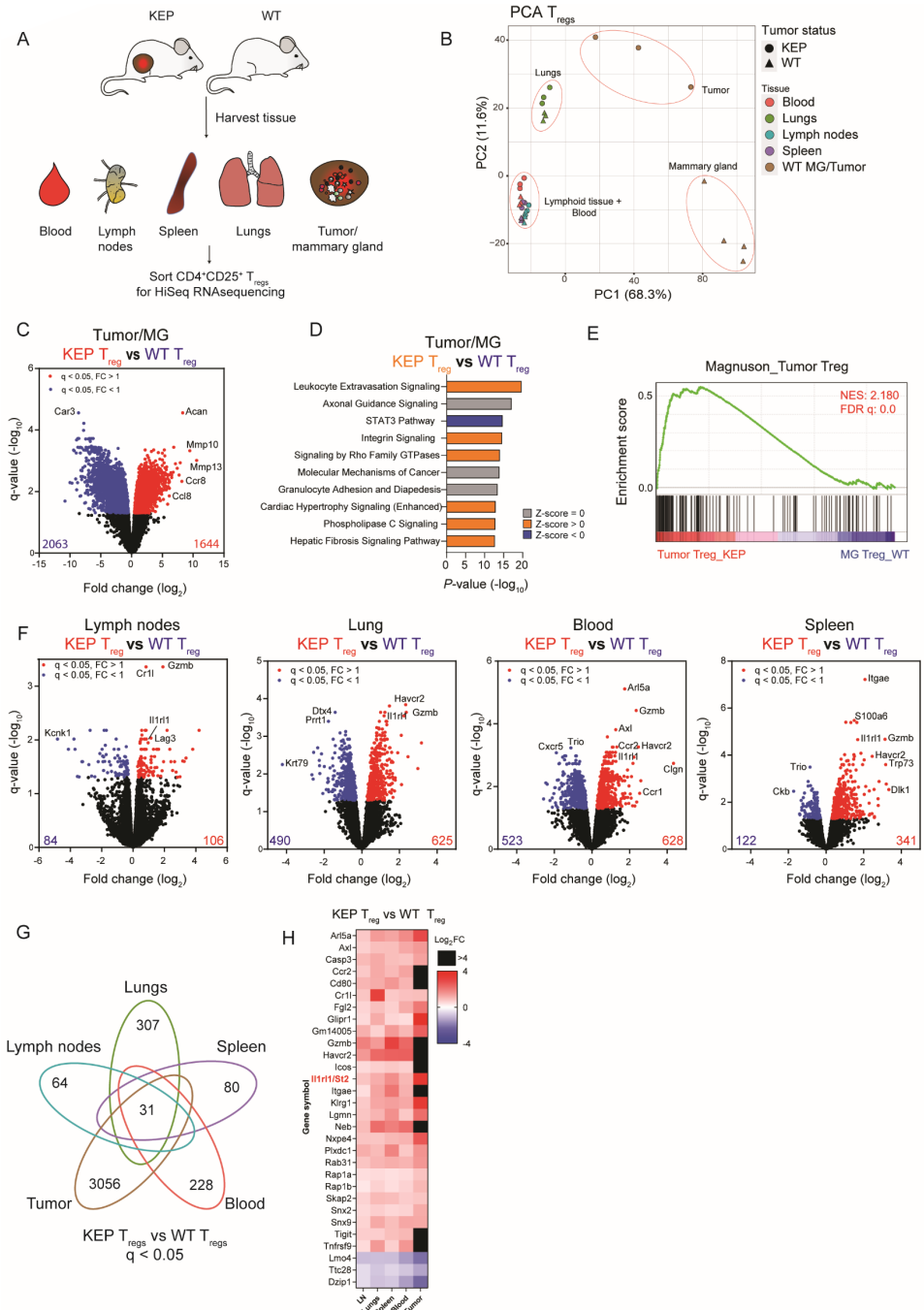


**FIGURE 2. Mammary tumor formation impacts T<sub>reg</sub> gene expression in distant sites.** **A.** Schematic overview of experiment. **B.** PCA plot of transcriptomic profiles of T<sub>regs</sub>. Each symbol represents one sample of sequenced T<sub>regs</sub>. **C.** Volcano plots showing differentially expressed genes (q<0.05) comparing T<sub>regs</sub> isolated from tumors of KEP mice versus healthy mammary gland of WT controls. **D.** IPA on differentially expressed genes (q<0.05) comparing T<sub>regs</sub> isolated from tumors of

KEP mice versus healthy mammary gland of WT controls. Top 10 statistically significant pathways are shown. **E.** GSEA comparing KEP/WT  $T_{regs}$  isolated from tumors and healthy mammary gland with TIT<sub>reg</sub> gene set (Magnuson et al., 2018). Normalized enrichment score (NES) and false discovery rate (FDR) indicated. **F.** Volcano plots showing differentially expressed genes ( $q < 0.05$ ) from  $T_{regs}$  isolated from indicated tissues of tumor-bearing KEP mice versus WT controls. Red indicates upregulated in KEP, blue indicates upregulated in WT. **G.** Venn diagram showing distribution of differentially expressed genes ( $q < 0.05$ ) identified by comparing gene expression of  $T_{regs}$  isolated of tumor-bearing KEP mice versus WT controls for each tissue. **H.** Heatmap depicting  $\text{Log}_2\text{FC}$  change of 30 shared KEP  $T_{reg}$  genes up/down regulated in KEP  $T_{regs}$  across tissue ( $q < 0.05$ , KEP  $T_{reg}$  versus WT  $T_{reg}$  per tissue).

### The impact of mammary tumorigenesis on $T_{regs}$ is dictated by the tissue context

In addition to transcriptional commonalities observed in KEP  $T_{regs}$  in distant organs, we identified a large number of tumor-induced genes in KEP  $T_{regs}$  that were not shared across multiple tissues, but rather dependent on the tissue-context (Fig. 2G), indicating that the local environment shapes the response of  $T_{regs}$  to mammary tumorigenesis. Therefore, we continued our characterization of  $T_{regs}$  in distant organs of tumor-bearing KEP mice by exploring the impact of the tissue-context. To do so, we omitted tumors and mammary glands from the dataset and re-analyzed the  $T_{reg}$  transcriptome. PCA analysis revealed that  $T_{regs}$  derived from the same tissues cluster together, indicating that tissue residence is a more dominant factor for the transcriptional state of  $T_{regs}$  than the presence or absence of a primary mammary tumor (Fig. 3A). To elaborate the relationship between  $T_{regs}$  in different tissues, we performed correlation analysis, and found  $T_{regs}$  from LNs, spleen and blood to be relatively closely correlated, whereas lung  $T_{regs}$  were very distinct (Fig. 3B). Interestingly, visualization of differentially regulated genes of matched tissues in a force-directed graph (KEP vs WT  $T_{regs}$ ,  $q < 0.05$ )<sup>33</sup> revealed complex relationships between clusters of genes dependent on the tissue context (Fig. 3C). Among these, roughly 30% of differentially regulated genes in KEP  $T_{regs}$  versus WT  $T_{regs}$  were found to be tissue specific (74/183 genes in LN, 379/1100 genes in lung, 417/1129 genes in blood, 107/462 genes in spleen), indicating that KEP  $T_{regs}$  in distant organs acquire a unique tissue-specific transcriptional profile (Fig. 3C, data file S1). We next performed IPA to interrogate which molecular pathways are associated with the differentially expressed genes between KEP and WT  $T_{regs}$  in distant organs. Notably, we identified several pathways related to T cell effector states (Th1 pathway, Th2 pathway, T helper cell differentiation, Th1 and Th2 Activation Pathway) to be shared among KEP  $T_{regs}$  in multiple distant organs (Fig. 3D). In addition to shared pathways, we also found several pathways that were only observed for specific tissues, such as “Integrin Signaling” in blood  $T_{regs}$  and “Apoptosis Signaling” in lung  $T_{regs}$ , highlighting the differential impact of mammary tumorigenesis on  $T_{regs}$  in distant organs.

Taken together, these data demonstrate that the mammary tumor-induced changes in  $T_{regs}$  are strongly influenced by their tissue context, raising the question whether these site-specific differences may have functional consequences for the progression of breast cancer.

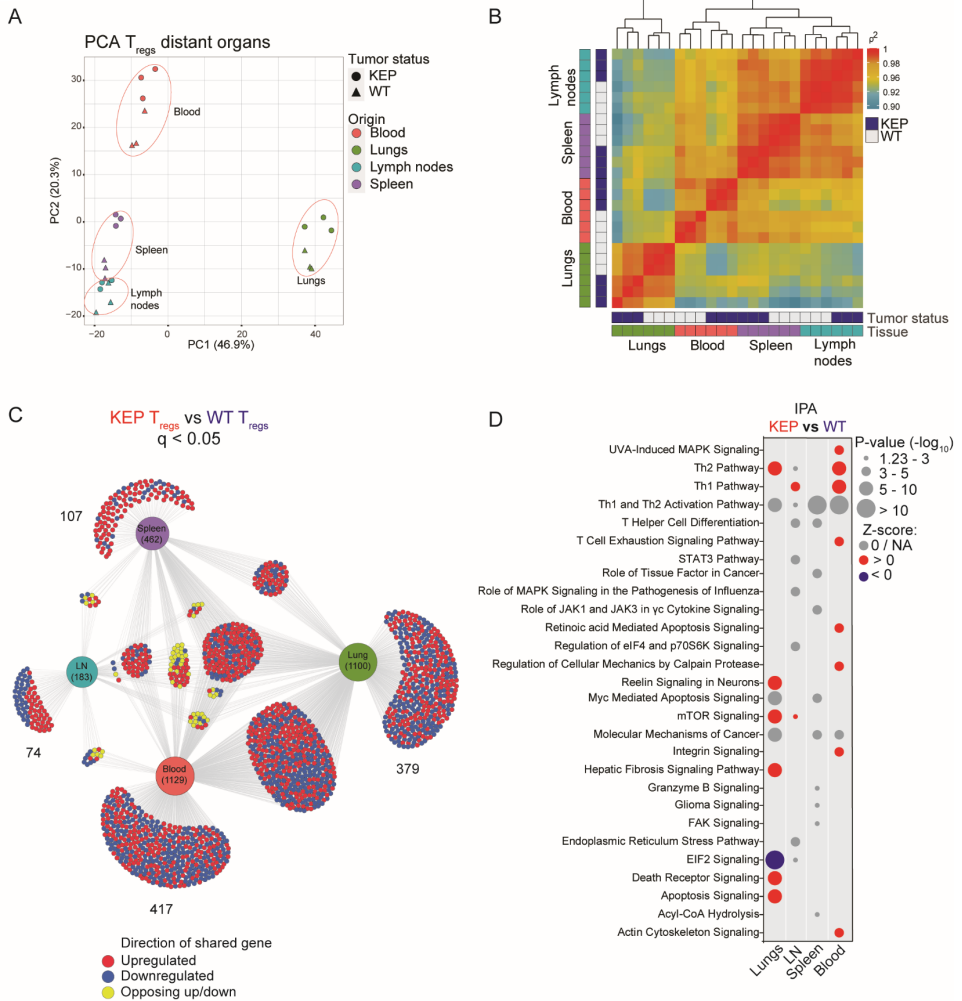


**FIGURE 3. Tissue-dependent transcriptional changes in KEP T<sub>regs</sub>.**

**A.** PCA plot of transcriptional profiles of T<sub>regs</sub> isolated from distant organs and blood of KEP mice bearing end-stage tumors versus healthy mammary gland of WT controls. **B.** Correlation plot matrix plot showing Spearman coefficient between transcriptional profiles of T<sub>regs</sub> isolated from distant organs and blood of KEP mice bearing end-stage tumors and WT controls. **C.** Force-directed graph depicting differentially expressed genes between KEP T<sub>regs</sub> vs WT T<sub>regs</sub> (q<0.05). Genes identified by comparing gene expression of T<sub>regs</sub> isolated from distant organs and blood of tumor-bearing KEP mice versus WT controls for each tissue, depicted by Divenn<sup>33</sup>. **D.** IPA on differentially expressed genes (q<0.05) comparing T<sub>regs</sub> isolated from indicated tissues of KEP mice bearing end-stage tumors versus WT controls. Top 10 significant pathways are shown for each tissue.

### **Tumor-educated $T_{regs}$ promote lymph node metastasis but not lung metastasis**

As we observed systemic and organ-specific mammary tumor-induced alterations of  $T_{regs}$ , we set out to explore the impact of  $T_{regs}$  on multi-organ metastatic disease utilizing the KEP-based mastectomy model of spontaneous breast cancer metastasis (Fig. 4A)<sup>25,34</sup>. In this model, after orthotopic transplantation of a KEP-derived tumor fragment followed by surgical removal of the outgrown tumor, mice develop overt multi-organ metastatic disease, mainly in Ax. TDLNs and lungs. Like primary tumor formation, metastatic disease is also accompanied by the accumulation of  $T_{regs}$ , with elevated expression of ICOS, CTLA4 and ST2, as compared to non-transplanted naïve controls (Fig. S3A-E).

To assess the functional significance of  $T_{regs}$  during early metastasis formation, we treated mice in the neoadjuvant setting with a recently developed Fc-modified antibody, targeting the IL2R $\alpha$  receptor, CD25 (anti-CD25-M2a), which has been described to efficiently and specifically deplete  $T_{regs}$  in tumors and peripheral tissue<sup>35</sup>. Indeed, anti-CD25-M2a treatment efficiently depleted FOXP3<sup>+</sup>CD4<sup>+</sup> T cells from tumors, spleen, lymph nodes, lungs and circulation in mice bearing transplanted KEP tumors (Fig. 4B-C, S3F-G). Depletion of  $T_{regs}$  was observed for up to 10 days after start of treatment in blood. Although anti-CD25-M2a treatment resulted in increased IFN $\gamma$  expression in both intratumoral CD4<sup>+</sup> and CD8<sup>+</sup> T cells (Fig. 4D), consistent with the concept that tumor-induced  $T_{regs}$  are immunosuppressive, we did not observe an effect on primary tumor growth (Fig. 4E). Similarly, depletion of  $T_{regs}$  in mammary tumor-bearing transgenic KEP mice did not affect primary tumor growth or survival (Fig. S3H).

After mastectomy, mice were monitored for the development of overt metastases. While neoadjuvant  $T_{reg}$  depletion did not improve metastasis-related survival or reduce the number of lung metastases (Fig. 4F, S3I), micro- and macroscopic analysis of Ax. TDLNs (Fig. S3J) revealed that anti-CD25-M2a treated mice developed significantly fewer LN metastases as compared to controls (Fig. 4G). The incidence of LN metastasis of control mice was 93% (14/15), which was reduced to 56% (9/16) upon anti-CD25-M2a treatment. No difference was observed in the size of LN metastases that did develop in both groups (Fig. S3K). The observation that  $T_{reg}$  depletion reduces the incidence of LN metastasis by ~50%, but does not affect lung metastasis, was consistent across four independent experimental KEP tumor donors, even though LN metastasis incidence of control groups varied between 41.67%-93.3% in a donor-dependent fashion (Fig. 4H-I). These findings indicate that  $T_{regs}$  promote metastasis formation, leading to increased incidence of LN metastasis, but also reveals that the impact of  $T_{regs}$  on metastasis formation is dependent on the tissue context since lung metastases remain unaffected.

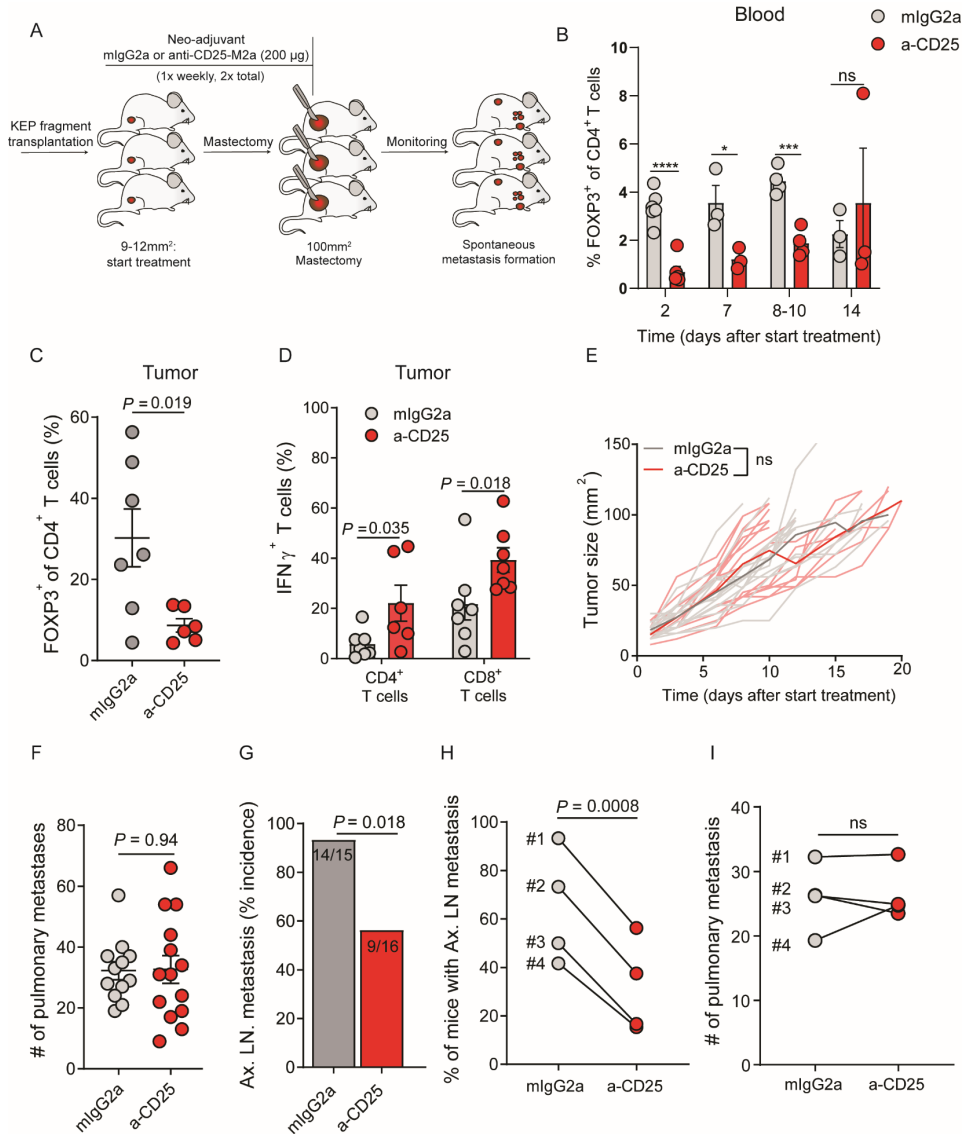


**FIGURE 4. Tumor-educated T<sub>regs</sub> promote lymph node metastasis but not lung metastasis**

**A.** Schematic overview of study. (n=15-16 mice/group). **B.** Frequency of FOXP3<sup>+</sup> cells of CD4<sup>+</sup> T cells in mice bearing transplanted KEP tumors, treated with mlgG2a or anti-CD25 at indicated timepoints after start of treatment. (n=3-6 mice/group). **C.** Intratumoral frequency of FOXP3<sup>+</sup> cells in mastectomized tumors, gated on live, CD45<sup>+</sup>, CD3<sup>+</sup>, CD4<sup>+</sup> T cells as determined by flow cytometry (n=6-7 mice/group). **D.** Frequency of IFN $\gamma$ <sup>+</sup> cells of CD4<sup>+</sup> and CD8<sup>+</sup> T cells, in 100mm<sup>2</sup> mastectomized KEP tumors of mice treated with neoadjuvant mlgG2a and anti-CD25 as determined by flow cytometry (n=6-7 mice/group) following a 3 hour ex vivo stimulation. **E.** Primary tumor growth kinetics of mice bearing transplanted KEP tumors, treated with mlgG2a or anti-CD25. **F.** Number of pulmonary metastases in mice treated with neoadjuvant mlgG2a and anti-CD25. (n=15-16 mice/group). **G.** % and number of mice with detectable micro/macroscopic metastases in Ax. TDLNs, in mice treated with neoadjuvant mlgG2a and anti-CD25. (n=15-16 mice/group). **H-I.** Ax. LN metastasis incidence (**H**) and # of lung metastases (**I**) of each independent experimental donor is shown, in mice receiving weekly neoadjuvant treatment of 200 µg mlgG2a or anti-CD25. Symbol indicates an experimental group (mlgG2a/a-CD25), each line

connects an independent experimental (donor #1 used in Fig. 4G, I n=15-16 mice/group, donor #2 used in Fig. 5A n=15-16, donor 3+4 used in Fig. 6A n=30-31 mice/group). Data in B-D, F show mean  $\pm$  S.E.M. P-values are determined by Unpaired Student's T-test (B,C,F), Mann-Whitney test (D), area under curve (AUC) calculation (E), Fisher's exact test (G), and Paired Student's T-test (H,I)

### **T<sub>regs</sub> differentially modulate NK cell activation in the lymph node and lung niche.**

To gain more insight into how T<sub>regs</sub> promote metastasis formation in Ax. LNs, we first explored the potential role of CD8<sup>+</sup> T cells in controlling LN metastasis formation upon T<sub>reg</sub> depletion, as we found that T<sub>regs</sub> suppress IFN $\gamma$  expression by CD8<sup>+</sup> T cells in the primary tumor microenvironment (Fig. 4D). To do so, we co-depleted CD8<sup>+</sup> T cells (Fig. S4A) and T<sub>regs</sub> in the KEP metastasis model, but did not find a difference in LN metastasis incidence between anti-CD25 and anti-CD25/CD8 treatment (Fig. 5A), suggesting that the reduced LN metastasis incidence upon depletion of T<sub>regs</sub> is not linked to intratumoral activation of CD8<sup>+</sup> T cells (Fig. 4D). Since we observed systemic activation and rewiring of highly immunosuppressive T<sub>regs</sub> in response to tumorigenesis, we next hypothesized that T<sub>regs</sub> may differentially facilitate metastasis formation through tissue-specific interactions in the local metastatic niche, independent of their activity in the primary tumor.

To study this as close to the *in vivo* situation as possible, we assessed the impact of tumor-educated T<sub>regs</sub> on immune cells with potential anti-tumor activity in Ax. TDLNs *in vivo*, instead of using traditional *in vitro* suppression assays in which cells may lose their functionality imposed by their respective tissue-microenvironment. *In vitro* suppression assays therefore fail to reproduce the complex interactions that exist *in vivo*, rendering these assays of limited value for studying metastatic niche-dependent processes. Instead, we depleted T<sub>regs</sub> in mice bearing transplanted KEP tumors and analyzed the phenotype and function of T- and NK cells in Ax. TDLNs compared to control treated and naïve mice when primary tumors reached a size of 100mm<sup>2</sup> *ex vivo*. We also analyzed T- and NK cells in tumors, blood and lungs, to gain insights into the tissue-specific impact of tumor-educated T<sub>regs</sub> on these cells. Interestingly, increased expression of the cytotoxic molecule granzyme B by NK cells (CD3<sup>-</sup>, NKp46<sup>+</sup>, DX5<sup>+</sup>) was observed in the Ax. TDLNs of tumor-bearing mice upon T<sub>reg</sub> depletion (Fig. 5B-C, S4B). Increased granzyme B expression was not observed in NK cells in lungs, blood and tumor upon T<sub>reg</sub> depletion despite higher baseline expression compared to Ax. TDLNs (Fig. S4C-E), indicating that tumor-activated T<sub>regs</sub> interfere with granzyme B expression of NK cells specifically in the Ax. LN niche. Next, we analyzed the surface expression of CD107a on NK cells as a readout for their degranulation, which is an important mechanism for NK cell cytotoxicity<sup>36</sup>. This showed that NK cells in Ax. TDLNs, but not lungs or Ax. NDLNs, from T<sub>reg</sub>-depleted mice cells have increased surface expression of CD107a compared to control treatment (Fig. 5D, S4F), showing that Ax. TDLN NK cells increase the release of intracellular granules upon T<sub>reg</sub> depletion *in vivo*. In *in vitro* stimulated NK cells, CD107a expression was not significantly affected by T<sub>reg</sub> depletion (Fig. S4G), suggesting that the impact of T<sub>regs</sub> on NK cell degranulation is not affecting their intrinsic capacity to degranulate under highly



stimulatory conditions, but is rather a result of T<sub>reg</sub>/NK cell interactions *in vivo*. In contrast, we did not find a significant effect of T<sub>reg</sub> depletion on T cells in terms of granzyme B, CD107a, IFN $\gamma$ , TNF $\alpha$  expression or IFN $\gamma$  by NK cells in Ax. TDLNs and lungs (Fig. S4H-L).

To further dissect the differential impact of T<sub>regs</sub> on NK cells in the LN and lung niche *in vivo*, we conducted bulk RNAseq analysis on FACS-sorted NK cells isolated from T<sub>reg</sub>-depleted and T<sub>reg</sub>-proficient tumor-bearing mice (Fig. 5E). Notably, anti-CD25 induces depletion of T<sub>regs</sub> via antibody-dependent cell-mediated cytotoxicity (ADCC) through engagement of Fc receptors<sup>35</sup> on innate effector cells, including NK cells<sup>37</sup>. To confirm that the observed activation of NK cells upon antibody-mediated depletion of T<sub>regs</sub> is independent of their role in ADCC, we now utilized *Foxp3*<sup>DTR-GFP</sup> mice in which FOXP3<sup>+</sup> cells are efficiently depleted upon injection of diphtheria toxin (DT) (Fig. S5A). NK cells were obtained from lungs and Ax. TDLNs of PBS or DT treated *Foxp3*<sup>DTR-GFP</sup> mice bearing transplanted KEP tumors. Gene expression analysis of NK cells from T<sub>reg</sub>-depleted versus T<sub>reg</sub> non-depleted mice identified 1036 and 646 genes to be differentially expressed in the LNs and lungs respectively, showing that the influence –directly, indirectly, or due to NK cell intrinsic differences- of T<sub>regs</sub> on the NK cell transcriptome, is more pronounced in Ax. TDLNs than in lungs (Fig. 5F-G, data file S2).

To identify which molecular pathways are controlled by T<sub>regs</sub> in NK cells in tumor-bearing mice, we performed GSEA analysis on the differentially expressed genes of both lung and Ax. TDLN NK cells from T<sub>reg</sub>-depleted versus T<sub>reg</sub> non-depleted mice using the MSigDB Hallmark Gene sets, which represent 50 well-defined biological processes<sup>38</sup> (Fig. 5H, S5B). We found that the depletion of T<sub>regs</sub> induces the upregulation of molecular pathways related to DNA replication (G2M checkpoint, E2F targets, mitotic spindle) and inflammation (inflammatory response, IFN $\gamma$  response) in both Ax. TDLN and lung NK cells, suggesting a common role of T<sub>regs</sub> in curbing NK cell proliferation and activation. However, we also identified pathways that were uniquely upregulated in either Ax. TDLN NK cells (IL6-JAK-STAT3 signaling, IL2-STAT5 signaling) or lung NK cells (Interferon alpha response, TNF $\alpha$  signaling via NF- $\kappa$ B). Although both Ax. TDLN and lung NK cells show signs of activation upon depletion of T<sub>regs</sub> based on GSEA, we identified 676 genes to be uniquely upregulated in Ax. TDLN NK cells of T<sub>reg</sub>-depleted versus T<sub>reg</sub>-non-depleted mice, compared to 326 in lung NK cells (Fig. 5I). Interestingly, a subset of genes found specifically upregulated in Ax. TDLN NK cells of T<sub>reg</sub>-depleted mice encodes for proteins with immunomodulatory properties that were not found in lung NK cells of T<sub>reg</sub>-depleted animals, including *Gzmb*, which we had previously identified in our FACS-based analyses of NK cells (Fig. 5B-C). Furthermore, we identified other genes encoding for proteins involved in cytotoxicity (*Gzma*, *Serp1nb9b*), migration (*Ccl4*, *Ccl8*, *Ccl22*, *Cxcr6*), co-stimulatory receptors (*Icosl*, *Tnfrsf4*), and co-inhibitory receptors (*Tigit*, *Lag3*, *Ctla4*, *Klrg1*), which are indicative of activated NK cells. In summary, these data show that T<sub>regs</sub> regulate NK cells in a tissue-specific manner, and suggest that tissue-context does not only drive T<sub>reg</sub> phenotype, but also impacts their interactions with target cells such as NK cells.

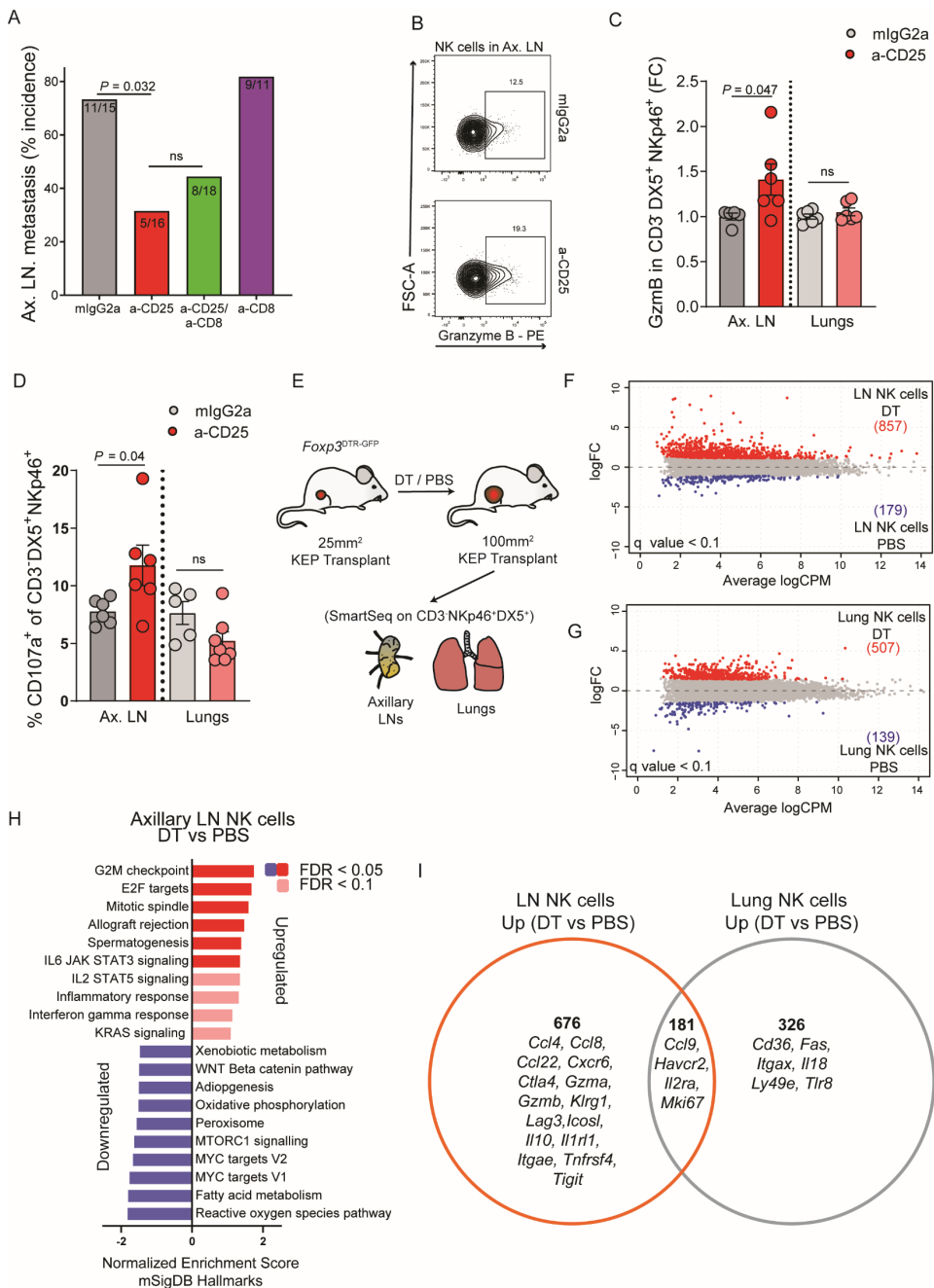


**FIGURE 5. T<sub>regs</sub> differentially impact NK cells in LN and lungs**

**A.** % and number of mice with detectable micro/macroscopic metastases in Ax. TDLNs, in mice treated with neoadjuvant indicated treatments. (n11-18 mice/group). **B.** Representative dot plot of granzyme B expression by NK cells in Ax. TDLNs of mice bearing 100mm<sup>2</sup> KEP tumors, treated with neoadjuvant mlgG2a or anti-CD25. **C.** Relative granzyme B expression by NK cells (CD3<sup>+</sup>DX5<sup>+</sup>NKp46<sup>+</sup>) in Ax. TDLNs and lungs of mice bearing 100mm<sup>2</sup> KEP tumors, treated with neoadjuvant mlgG2a or anti-CD25,

following a 3 hour ex vivo stimulation (n=6 mice/group). Data are normalized to % GzmB<sup>+</sup> of NK cells of control mlgG2a treated mice. **D.** CD107a expression of NKp46<sup>+</sup>DX5<sup>+</sup> NK cells from Ax. TDLNs and lungs of mice bearing transplanted KEP tumors (100mm<sup>2</sup>) receiving weekly neoadjuvant treatment of 200µg anti-CD25 or mlgG2a (n=6/group). **E.** Schematic overview of study. Mice received treatment at t=0 and t=7. (n=4 mice/group). **F-G** MA plot of differentially regulated transcripts for Ax. TDLN NK cells (**F**), and lung NK cells (**G**) DT versus PBS treatment. Significantly different transcripts are labelled in red (up), and blue (down). **H.** GSEA analysis of Ax. TDLN NK cells, DT vs PBS, using hallmark gene sets. Top 10 enriched up- and downregulated pathways are shown. **I.** Venn diagram depicting distribution of upregulated genes (q < 0.1) between Ax. TDLN and lung NK cells DT versus PBS treatment. Data in C-D show mean ± S.E.M. P-values are determined by Mann-Whitney Test (C-D) and Fisher's Exact test (A).

### T<sub>regs</sub> promote metastasis through inhibition of NK cells in the lymph node niche

We next assessed whether the inhibitory effect of T<sub>regs</sub> on Ax. TDLN NK cells impacts their capacity to control LN metastasis formation. We performed neoadjuvant co-depletion of T<sub>regs</sub> using anti-CD25-M2a and NK cells using anti-NK1.1 in the KEP metastasis model. Anti-NK1.1 efficiently depleted NKp46<sup>+</sup>DX5<sup>+</sup> NK cells in the blood of KEP tumor-bearing mice (Fig. S5C). Strikingly, whereas depletion of T<sub>regs</sub> significantly reduced the incidence of Ax. LN metastasis, combined depletion of T<sub>regs</sub> and NK cells completely restored LN metastasis formation (Fig. 6A). Anti-NK1.1 alone did not alter LN metastasis incidence and none of the treatments affected the number of lung metastases (Fig. 6B). Combined, our findings show that tumor-educated T<sub>regs</sub> repress NK cell activation in Ax. TDLNs, thereby curbing their anti-metastatic potential, leading to an increased incidence of LN metastasis. This T<sub>reg</sub>-mediated immune escape mechanism is specific to the Ax. LN, as T<sub>regs</sub> did not control lung metastasis in this model. Because we did observe some activation of lung NK cells at the transcriptional level in T<sub>reg</sub>-depleted versus non-depleted mice (Fig. 5I), we hypothesized that additional layers of immunosuppression in the lung microenvironment that are independent of T<sub>regs</sub> may hinder the anti-metastatic potential of lung NK cells. In support of this hypothesis, we found that lung NK cells are mostly terminally differentiated (CD27<sup>-</sup>CD11b<sup>+</sup>) in tumor-free mice, but undergo a partial shift towards a non-cytotoxic immature phenotype (CD27<sup>+</sup>CD11b<sup>-</sup>) in tumor-bearing mice, independent of T<sub>regs</sub> (Fig. S5D). In contrast to lungs, and in line with previous literature<sup>39,40</sup>, Ax. TDLN NK cells were found to be mostly in CD27<sup>+</sup>CD11b<sup>-</sup> (immature) and CD27<sup>+</sup>CD11b<sup>+</sup> (cytotoxic) states (Fig. S5E), highlighting the differences between NK cells in LNs and lung. Importantly, maturation status in Ax. TDLN NK cells was not affected in tumor-bearing mice, suggesting this mechanism is specific to lungs, and potentially contributes to observed differences between lung and LN.

### Reduced NK cells versus increased T<sub>regs</sub> in sentinel lymph nodes of breast cancer patients

Finally, we validated our preclinical findings on T<sub>reg</sub> and NK cell interactions in the lymph node niche of breast cancer patients. To do so, we analyzed the accumulation of T<sub>regs</sub> (CD4<sup>+</sup>CD25<sup>high</sup>FOXP3<sup>+</sup>) and NK cells (CD56<sup>+</sup>CD16<sup>-</sup> and CD56<sup>low</sup>CD16<sup>+</sup>) in tumor-free and tumor-positive sentinel LNs of breast cancer patients (BrCa SLN<sup>-</sup>/SLN<sup>+</sup>), and in Ax. LNs from

healthy controls (HLNs), using a previously described flow cytometry dataset<sup>14</sup>. In line with previous analyses of this unique dataset<sup>14</sup> and consistent with our preclinical data (Fig. 1C),  $T_{reg}$  levels are significantly elevated in BrCa SLNs as compared to HLNs (Fig. 6C). We also observed a statistically significant reduction of  $CD56^{low}CD16^{+}$ , but not  $CD56^{+}CD16^{-}$  NK cells in BrCa SLN-, and a similar trend in BrCa SLN+ (Fig. 6D-E). Notably, in particular  $CD56^{low}CD16^{+}$  have been described to have cytotoxic activity<sup>41</sup>. Combined, this shifts the  $T_{reg}/NK$  cell ratio strongly towards  $T_{regs}$  in both tumor-free and tumor-positive BrCa SLNs compared to HLNs (Fig. 6F). Despite the low number of BrCa SLN+ samples, we also observed a non-significant trend of a higher  $T_{reg}/NK$  cell ratio in SLN+ versus SLN- samples. A rise in  $T_{regs}$  in conjunction with a reduction of potentially cytotoxic NK cells in the SLN niche is in accordance with our preclinical finding that LN NK cells have reduced expression of CD107a and the cytotoxic molecule granzyme B under control of  $T_{regs}$  in tumor-bearing mice (Fig. 5B-D).

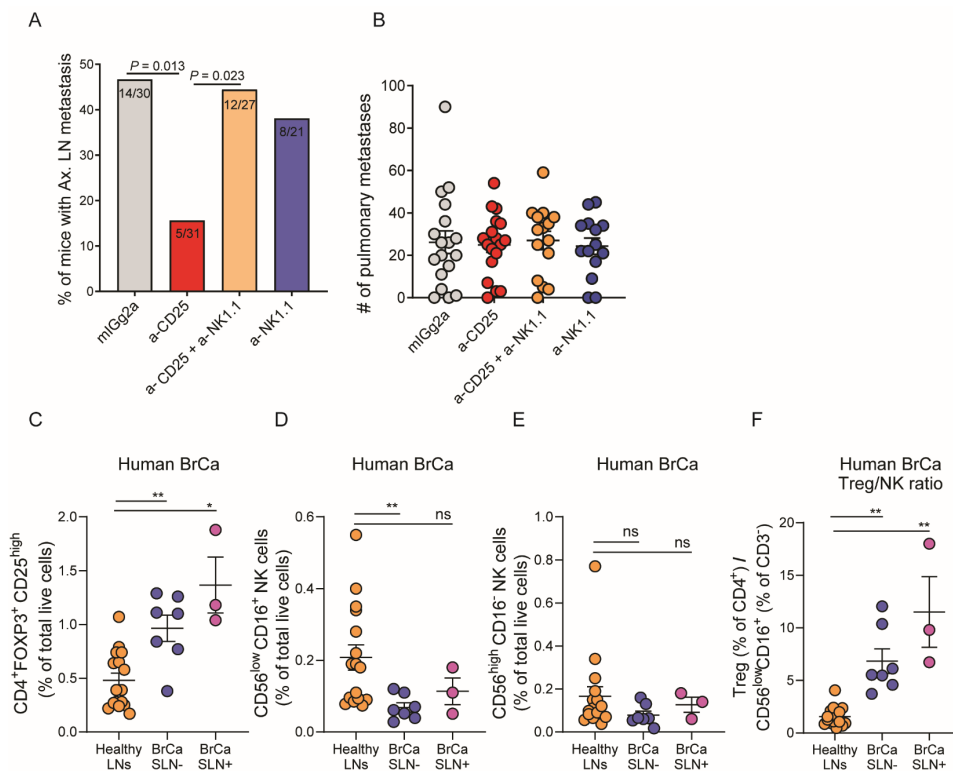


**FIGURE 6.  $T_{regs}$  promote axillary LN metastasis through inhibition of NK cells.**

**A.** % and number of mice with detectable micro/macrosopic metastases in Ax. TDLNs, in mice receiving neoadjuvant treatment as indicated. (n=21-31 mice/group, data pooled from two independent experiments). **B.** Number of pulmonary metastases in mice receiving indicated neoadjuvant treatment. (n=14-16 mice/group). **C.** Frequencies of  $CD3^{+}CD4^{+}CD25^{+}FOXP3^{+}$  cells of total live cells in human HLNs (n=16), BrCa tumor-negative (n=7) and tumor-positive (n=3) SLNs. **D-E.** Frequencies of indicated subset of NK cells of total live cells in human HLNs (n=16), BrCa tumor-negative (n=7) and tumor-positive (n=3) SLNs. **F.** Ratio of  $T_{reg}$  (% of  $CD4^{+}$ ) versus  $CD56^{low}CD16^{+}$  (% of  $CD3^{+}$ ) in human HLNs

(n=16), BrCa tumor-negative (n=7) and tumor-positive (n=3) SLNs. Data in B-F show mean  $\pm$  S.E.M. P-values are determined by Kruskal-Wallis test with Dunn's correction for multiple comparisons (C-F), Fishers Exact test (A). \*\* P < 0.01, \*\*\* P < 0.001, \*\*\*\* P < 0.0001

## DISCUSSION

Understanding the nature of cancer-associated systemic immunosuppression and its impact on different (pre-)metastatic niches is essential to ultimately design effective therapeutic strategies that prevent or fight metastatic disease. Here, we show that mammary tumorigenesis has an extensive impact on T<sub>regs</sub>, both intratumorally and in distant organs. Tumor-educated T<sub>regs</sub> are highly activated and immunosuppressive, and display tissue-specific adaptation to tumor development. This has functional relevance for metastasis formation, as T<sub>regs</sub> selectively promote LN metastasis, but not lung metastasis, through inhibition of NK cells. These data highlight the importance of the tissue-context for immune escape mechanisms, and reveal a causal role for T<sub>regs</sub> in the development of LN metastasis. An extensive number of clinical studies has reported that high infiltration of FOXP3<sup>+</sup> TILs in either primary breast tumors or Ax. LNs is associated with an increased incidence of LN metastasis, across breast cancer subtypes<sup>14–16,42</sup>. As five-year survival of breast cancer patients with LN involvement is up to 40% lower than node-negative patients<sup>43,44</sup>, it is of crucial importance to understand the potential role of T<sub>regs</sub> in the development of LN metastasis. Interestingly, one study of which we have further explored the dataset here, showed that T<sub>regs</sub> are not only increased in sentinel LNs with metastatic involvement, but also accumulate in non-invaded sentinel LNs compared to LNs from healthy women, suggesting T<sub>reg</sub> accumulation precedes LN metastasis formation<sup>14</sup>. Recently, others have studied the phenotype of T<sub>regs</sub> in LNs of breast cancer patients and showed that T<sub>regs</sub> acquire an increased effector-like phenotype in tumor cell-invaded versus non-invaded LNs<sup>17</sup>. These data are in line with our observations that T<sub>regs</sub> in LNs are increased and activated in the context of mammary tumorigenesis. So far, clinical correlations between T<sub>regs</sub> and breast cancer metastasis to other anatomical sites have not been reported, which suggest that T<sub>regs</sub> may play a unique role in the formation of LN metastasis, as supported by our data.

NK cells are a well-recognized key element of the anti-tumor response<sup>45,46</sup>, but the role and cellular crosstalk of NK cells in the context of lymph node metastasis has remained unclear. Here, we show that NK cells in Ax. TDLNs have anti-metastatic potential, provided they are relieved from the immunosuppressive pressure by T<sub>regs</sub>. The relevance of these findings for human breast cancer is supported by our observation that the T<sub>reg</sub>/NK cell ratio strongly shifts towards T<sub>regs</sub> in SLNs of BrCa patients compared to healthy LNs. In addition, an explorative study using metastatic LNs from melanoma patients showed that *ex vivo* depletion of T<sub>regs</sub> enhanced cytolytic activity of LN NK cells *in vitro*, suggesting T<sub>regs</sub> can also inhibit LN NK cells in melanoma<sup>47</sup>. For breast cancer specifically, the expression

of granzyme B within tumor-infiltrating NK cells was found to negatively correlate to  $T_{reg}$  accumulation<sup>48</sup>. Furthermore, another recent study identified that clearance of Ax. LN metastasis in breast cancer patients treated with neoadjuvant chemotherapy significantly correlated with increased cytotoxic potential of NK cells in peripheral blood as well as with decreased intratumoral CTLA4 gene expression<sup>49</sup>, which is well known to be important for  $T_{reg}$  immunosuppression<sup>50</sup>.

Our findings demonstrate that  $T_{regs}$  show tissue-dependent rewiring in response to mammary tumorigenesis, which may either be explained through tissue-specific upstream regulators, or is reflective of the distinct inherent differences between tissue-resident  $T_{regs}$ , in particular in lymphoid versus non-lymphoid organs. Tissue-context does not only drive  $T_{reg}$  phenotype in tumor-bearing hosts, but also dictates the interaction between  $T_{regs}$  and one of their cellular targets, NK cells. Specifically, we found  $T_{reg}$  depletion to differentially affect lung and LN NK cells at both the transcriptional and the protein level (Fig. 5). Although transcriptomic analyses revealed that LN and lung NK cells acquire a more activated phenotype upon  $T_{reg}$  depletion, we found this to unleash NK-cell mediated anti-metastatic activity only in the lymph node niche, but not the lungs. We speculate that this may occur through the induction of an effector mechanism observed specifically in LN- but not lung- NK cells, such as increased expression of; the cytotoxic molecules granzyme A and B, NK cell co-stimulatory receptors, or chemokine receptors (Fig. 5I). Whether these specific phenotypic alterations observed in LN NK cells upon  $T_{reg}$  depletion are intrinsic to LN NK cells, or due to a unique feature of tumor-educated  $T_{regs}$  in TDLNs, remains to be elucidated. Alternatively, NK cells may be functionally repressed through other immunosuppressive mechanisms that are independent of  $T_{regs}$ , and specific to the lung niche. For example, we observed that lung, but not LN NK cells undergo a shift towards a more immature state in tumor-bearing mice (Fig. S5D-E). This occurs independent of  $T_{regs}$ , and potentially impacts their anti-metastatic potential. In line with this hypothesis, a recent study revealed that lung NK cells are suppressed by IL-33 activated innate lymphoid type 2 cells, which stunts their ability to control pulmonary metastasis of intravenously injected B16F10 cells<sup>51</sup>. This shows that NK cells can be suppressed beyond the control of  $T_{regs}$  in the lungs, highlighting the importance of local, tissue-specific mechanisms of immunosuppression and cancer immune surveillance during metastasis formation. Finally, NK cells may be functionally irrelevant for lung metastasis formation in this model independent of their activation status, through cancer cell-intrinsic differences between lymph- and lung metastasizing cancer cells that impacts their likelihood to be killed by NK cells<sup>45,52</sup>, which we have not explored in this study.

The lack of  $T_{reg}$ -mediated promotion of lung metastasis formation is seemingly in contrast with studies in the 4T1 breast cancer model where  $T_{regs}$  have been shown to promote lung metastasis<sup>22,23</sup>. An important difference between these studies and our study is that 4T1 primary mammary tumors respond to  $T_{reg}$  depletion, resulting in attenuation of tumor

growth<sup>22,23</sup>, while both spontaneous- and transplanted primary KEP mammary tumors do not respond to T<sub>reg</sub> depletion (Fig. 4E, S3H). It was recently reported that the reduction in lung metastasis upon T<sub>reg</sub> depletion in 4T1-bearing mice is a consequence of the primary tumor responding to T<sub>reg</sub> depletion, and not an effect of T<sub>regs</sub> on metastatic colonies in the lung niche<sup>23</sup>. In fact, an important conclusion from this study was that lung metastases are not effectively controlled after T<sub>reg</sub> depletion<sup>23</sup>, in line with our findings that metastasis to the lungs is not influenced by T<sub>regs</sub>. Furthermore, syngeneic cell lines like 4T1 poorly reflect the immunogenicity of human tumors of the same origin<sup>53</sup>. Recent research has shown that syngeneic cell lines derived from GEMMs show key differences in their immune landscape, with increased frequencies of T<sub>regs</sub>, CD8<sup>+</sup> T cells and NK cells, as compared to primary tumors in GEMMs<sup>54</sup>. These differences in immune landscape may critically impact the outcome of immunological studies, and thereby reduce their clinical value as compared to GEMM-based models such as the KEP model.

Despite observations that exogenous IL-33 can induce acute peripheral accumulation of ST2<sup>+</sup> T<sub>regs</sub><sup>55</sup> we find that blockade of endogenous IL-33 does not affect tumor-induced systemic T<sub>reg</sub> accumulation or proliferation (Fig. S2F-I), suggesting that T<sub>reg</sub> expansion in mammary tumor-bearing mice is regulated independent of IL-33, and thus remains an avenue of future research. Our *in vitro* studies (Fig S1L) suggest that a soluble factor in KEP serum can promote T<sub>reg</sub> survival. An important cytokine involved in T<sub>reg</sub> proliferation and survival<sup>56</sup> that we did not study here is IL-2. Therefore, future studies may analyze whether IL-2 is differentially expressed or regulated in tumor-bearing hosts, and might contribute to T<sub>reg</sub> expansion, as has been observed in tumor-bearing mice treated with recombinant IL-2<sup>56</sup>.

In conclusion, these findings reveal a causal role for T<sub>regs</sub> in the formation of LN metastasis through local suppression of NK cells, and may form the basis for the design of neoadjuvant therapeutic strategies aimed to reduce nodal metastasis in breast cancer patients.

### Limitations of the study

Although the use of a spontaneous GEMM-derived metastasis model increases the translational value of our findings, the absence of similar models for multi-organ spontaneous metastasis pose the experimental limitation of validation in comparable models. It will be relevant to extend our findings to similar models, when these are generated in the future. Another possible limitation is the analysis of T<sub>reg</sub> populations by bulk RNAseq. This technique provides limited insight into changes occurring in different T<sub>reg</sub> subpopulations within one tissue. Future studies may explore the distant impact of tumors on T<sub>regs</sub> more deeply using single-cell RNAseq or related techniques. Finally, we have not uncovered the molecular basis of tumor-induced T<sub>reg</sub> expansion, or precise T<sub>reg</sub>-NK cell interactions in the TDLN. Thus, a deeper investigation in this direction is an important avenue of future research.

### **Acknowledgements**

We acknowledge Alexander Rudensky for providing the IRES-DTR-GFP construct, Dr. Emiel J. Th. Rutgers and Dr. Petrousjka van den Tol for provision of clinical samples, and members of the Tumor Biology & Immunology Department, NKI for their insightful input. We thank the flow cytometry facility, genomics core facility, animal laboratory facility, transgenesis facility and animal pathology facility of the Netherlands Cancer Institute for technical assistance. This research was funded by NWO Oncology Graduate School Amsterdam (OOA) Diamond Program (KK), Netherlands Organization for Scientific Research grant NWO-VICI 91819616 (KEdV), Dutch Cancer Society grant KWF10083; KWF10623; KWF13191 (KEdV), KWF VU2015-7864 (RvdV, TDdG, KEdV) Oncode Institute (KEdV), and A Sister's Hope (TDdG). Components of the graphical abstract were prepared using Servier Medical Art, licensed under Creative Commons Attribution 3.0 Unported License.

### **Author contributions**

KK and KEdV conceived the ideas and designed the experiments. KK performed experiments and data analysis. MAA performed bioinformatical analyses. MDW, WP, AvW, DD generated data. KK, DK, KV, C-SH, and LR performed animal experiments. SAQ and RB provided a-CD25-M2A and IL33Trap respectively. RvdV, KvP, TDdG collected samples and generated human data. KEdV supervised the study, KEdV and KK acquired funding, KK and KEdV wrote the paper and prepared the figures with input from all authors.

### **Declaration of Interests**

KEdV reports research funding from Roche/Genentech and is consultant for Macomics outside the scope of this work. RvdV reports research funding from Genmab. TDdG received research support from Idera Pharmaceuticals, advisory/consultancy fees from LAVA Therapeutics, Parner Therapeutics, and Immunicum, and owns stock from LAVA Therapeutics.

## **MATERIAL AND METHODS**

### **RESOURCE AVAILABILITY**

#### **Lead contact**

Further information and requests for resources and reagents should be directed to and will be fulfilled by the lead contact, Karin. E. de Visser (K.d.visser@nki.nl).

#### **Materials availability**

All reagents generated in this study are available upon request with a completed material transfer agreement.



## Data and code availability

Bulk T<sub>reg</sub> and NK RNA-sequencing data have been deposited in the GEO and are publicly available as of the date of publication. Accession numbers are listed in the key resources table.

This paper does not report original code.

Any additional information required to reanalyze the data reported in this paper is available from the lead contact upon request.

## EXPERIMENTAL MODEL AND SUBJECT DETAILS

### Mice

The generation and characterization of genetically engineered mouse models for spontaneous mammary tumorigenesis has been described before<sup>24,57-60</sup>. The following mice have been used in this study: *Keratin14 (K14)-cre;Cdh1<sup>F/F</sup>;Trp53<sup>F/F</sup>*, *Whey Acidic Protein (Wap)-cre;Cdh1<sup>F/F</sup>;Pik3ca<sup>E545K</sup>*, *(Wap)-cre;Cdh1<sup>F/F</sup>;Pik3ca<sup>H1047R</sup>*, *Wap-cre;Cdh1<sup>F/F</sup>;Pten<sup>F/F</sup>*, *Wap-cre;Cdh1<sup>F/F</sup>;Akt<sup>E17K</sup>*, *Brca1<sup>F/F</sup>;Trp53<sup>F/F</sup>* (generous gift of Jos Jonkers, NKI) and *Cdh1<sup>F/F</sup>;Trp53<sup>F/F</sup>;Foxp3<sup>GFP-DTR</sup>* mice (further referred to as *Foxp3<sup>GFP-DTR</sup>*). All mouse models were on FVB/n background, and genotyping was performed by PCR analysis on toe clips DNA as described<sup>24</sup>. Starting at 6-7 weeks of age, female mice were monitored twice weekly for the development of spontaneous mammary tumor development. Tumors in *Brca1<sup>F/F</sup>;Trp53<sup>F/F</sup>* mice were somatically induced through intraductal delivery of lentiviral-Cre as described before<sup>58,59</sup>. Mice were monitored twice weekly for spontaneous mammary tumor development starting 6 weeks after intraductal delivery of lenti-viral Cre. Upon mammary tumor formation, perpendicular tumor diameters were measured twice weekly using a caliper. In all models, end-stage was defined as cumulative tumor burden of 225mm<sup>2</sup>. Age-matched WT littermates were used as controls.

Mice were kept in individually ventilated cages at the animal laboratory facility of the Netherlands Cancer Institute under specific pathogen free conditions. Food and water were provided *ad libitum*. All animal experiments were approved by the Netherlands Cancer Institute Animal Ethics Committee, and performed in accordance with institutional, national and European guidelines for Animal Care and Use. The study is compliant with all relevant ethical regulations regarding animal research.

### Patients

The mean age of the ten female patients at the time of SLN procedure was 56.3 years. Patients had either lobular (n=2) or ductal (n=6) carcinoma of the breast, one patient had a tumor that was classified as ductal/lobular and one patient a tumor that was classified as mucinous adenocarcinoma. One patient, who was diagnosed with two invasive breast

tumors (ductal), had both a luminal A (Her2-, ER+, PR+) and a luminal B Her2+ (Her2+, ER-, PR-) tumor. All other patients were diagnosed with hormone receptor expressing (Her2-, ER+, PR+) tumors, of which six were classified as luminal A and three as luminal B. The study was approved by the Institutional Review Board (IRB) of the VU University medical center and SLN samples were collected and handled according to guidelines described in the Code of Conduct for Proper Use of Human Tissue of the Dutch Federation of Biomedical Scientific Societies with written informed consent from the patients prior to SLN sampling.

## METHOD DETAILS

### Generation of *Foxp3*<sup>GFP-DTR</sup> mice

*Cdh1*<sup>F/F</sup>;*Trp53*<sup>F/F</sup>;*Foxp3*<sup>GFP-DTR</sup> mice (further referred to as *Foxp3*<sup>GFP-DTR</sup>) were generated using the previously described IRES-DTR-GFP targeting construct<sup>61</sup> (generous gift of Prof. Alexander Rudensky, MSKCC). Notably, Cre-recombinase is not expressed in *Foxp3*<sup>GFP-DTR</sup> mice, and generation of *Foxp3*<sup>GFP-DTR</sup> mice within the *Cdh1*<sup>F/F</sup>;*Trp53*<sup>F/F</sup> background matches the background of control (*Cdh1*<sup>F/F</sup>;*Trp53*<sup>F/F</sup>) mice used throughout the manuscript. The linearized IRES-DTR-GFP construct was introduced in the 3' untranslated region of *Foxp3* upstream of the polyadenylation signal in *Cdh1*<sup>F/F</sup>;*Trp53*<sup>F/F</sup> (FVB) embryonic stem cells (ESC) by electroporation as described before<sup>61,62</sup>. Neomycin-resistant clones were screened by PCR across the 3' arm. Correct targeting of the construct was confirmed by Southern blot. Correctly targeted clones were transfected with a FLP-deleter plasmid for excision of the PGK-Neo cassette. Transfected clones were selected by puromycin, and loss of the PGK-Neo cassette was confirmed by PCR. Selected ESCs were injected into C57BL/6N blastocysts and chimeric male offspring were mated to *Cdh1*<sup>F/F</sup>;*Trp53*<sup>F/F</sup> mice. Homozygous *Cdh1*<sup>F/F</sup>;*Trp53*<sup>F/F</sup>;*Foxp3*<sup>GFP-DTR</sup> females were used for experiments.

### KEP metastasis model

The KEP metastasis model has been applied as previously described<sup>25</sup>. Tumors from KEP mice (100mm<sup>2</sup>) were fragmented into small pieces (~1 mm<sup>2</sup>) and stored at -150 °C in Dulbecco's Modified Eagle's Medium F12 containing 30% fetal calf serum and 10% dimethyl sulfoxide. Selection of mouse invasive lobular carcinomas (mILC) donor tumors was based on high cytokeratin 8 and absence of vimentin and E-cadherin expression as determined by immunohistochemistry. Donor KEP tumor pieces were orthotopically transplanted into the 4<sup>th</sup> mammary fat pad of female recipient 9-12 week old WT FVB/n mice (Janvier). Upon tumor outgrowth to a size of 100mm<sup>2</sup>, donor tumors were surgically removed. Following mastectomy, mice were monitored for development of overt multi-organ metastatic disease by daily palpation and observation of physical health, appearance, and behavior. Lungs, liver, spleen, intestines, mesenterium, kidneys, adrenal glands, and tumor-draining (subiliac, proper axillary and accessory axillary) and distant LNs (mesenteric, renal, and caudal) were collected and analyzed microscopically for the presence of metastatic foci by immunohistochemical cytokeratin 8 staining. Macroscopically overt metastases were

collected separately for further analysis. Mice were excluded from analysis due to following predetermined reasons: No outgrowth of tumors upon transplantation, mice sacrificed due to surgery-related complications, mice sacrificed due to development of end-stage (225mm<sup>2</sup>) local recurrent tumors prior to presentation of metastatic disease.

### Murine intervention studies

Antibody treatments were initiated at tumor sizes of 25-45mm<sup>2</sup> (as indicated) in spontaneous mammary tumor-bearing KEP and *Foxp3*<sup>GFP-DTR</sup> mice, and at 12-20mm<sup>2</sup> in the KEP metastasis model (neoadjuvant setting). Mice were randomly allocated to treatment groups upon presentation of mammary tumors of indicated size. Tumor development in KEP mice prevented full blinding to genotypes during mouse handling, but researchers were blinded to treatment and genotype during cell, tissue and immunohistological analysis. Mice were intraperitoneally injected with: Fc-receptor optimized anti-CD25 (Clone M2a<sup>35</sup> 200 µg weekly for 2 weeks; mIgG2a control antibody 200 µg weekly for 2 weeks (C1.18.4, BioXcell); anti-mouse CD8α single loading dose of 400 µg, followed by 200 µg thrice a week (2.43, BioXcell); anti-mouse NK1.1, single loading dose of 400 µg, followed by 200 µg twice a week (PK136, BioXcell); Difteria Toxin (Sigma) 25 µg twice total (t = 0, t = 7 days); anti-mouse IL-33 (R&D systems) 3.75 µg thrice a week for 2 weeks; IL-33Trap<sup>32</sup> 50 µg daily for 1 week. Animal sample size for intervention studies was determined by power analysis using G\*power software, using effect sizes obtained from historical experiments or preliminary data. Due to the spontaneous nature of the used animal models for primary tumor formation and metastasis, cohorts were sequentially completed and analyzed in succession, similar in set up to clinical trials. In the KEP metastasis model, treatments were discontinued upon mastectomy. For survival curve experiments and end-stage analyses in KEP mice, antibody treatment continued until the tumor or the cumulative tumor burden reached 225mm<sup>2</sup>. For KEP intervention and KEP metastasis experiments, the following end points were applied according to the Code of Practice Animal Experiments in cancer research: (metastatic) tumor size > 225mm<sup>2</sup>, >20% weight loss since start of experiment, respiratory distress upon fixation, severe lethargy, (metastatic) tumor causing severe clinical symptoms as a result of location, invasive growth or ulceration.

### Preparation of single cell suspensions

For flow cytometry based analysis and cell sorting for *in vitro* assays and RNA sequencing, single cell suspensions were prepared from freshly isolated mouse tissues. Mice were sacrificed at indicated time points. KEP tumors, healthy mammary glands spleens and LNs were prepared as previously described<sup>63</sup>. In brief, tumors and mammary glands were mechanically chopped using the Mcllwain tissue chopper (Mickle Laboratory Engineering) and enzymatically digested with 3 mg ml<sup>-1</sup> collagenase type A (Roche) and 25 µg ml<sup>-1</sup> DNase I (Sigma) in serum-free medium for 1 h at 37°C in a shaking water bath. Enzyme activity was neutralized by addition of cold DMEM/8% FCS and suspension was dispersed

through a 70  $\mu\text{m}$  cell strainer. Lungs were perfused with ice-cold PBS *post mortem* to flush blood. Next, lungs were cut into small pieces and mechanically chopped using the Mcllwain tissue chopper. Lungs were enzymatically digested in 100  $\mu\text{g}/\text{mL}$  Liberase Tm (Roche) under continuous rotation for 30 minutes at 37  $^{\circ}\text{C}$ . Enzyme activity was neutralized by addition of cold DMEM/8% FCS and suspension was dispersed through a 70  $\mu\text{m}$  cell strainer. Spleens and lymph nodes were collected in ice-cold PBS, and dispersed through a 70  $\mu\text{m}$  cell strainer. Blood was obtained via cardiac puncture for end-stage analyses, and via tail vein puncture for time point analyses and collected in tubes containing heparin. Erythrocyte lysis for blood, spleen and lungs was performed using  $\text{NH}_4\text{Cl}$  erythrocyte lysis buffer for 2x5 (blood) and 1x1 (spleen, lungs) minutes.

### Flow cytometry: analysis and cell sorting

Single cell suspensions of human and murine samples were incubated in anti-CD16/32 (2.4G2, BD Biosciences) to block unspecific Fc receptor binding for 5 minutes. Next, cells were incubated for 20 minutes with fluorochrome conjugated antibodies diluted in FACS buffer (2.5% FBS, 2 mM EDTA in PBS). For analysis of nuclear transcription factors, cells were fixed and permeabilized after surface and live/dead staining using the FOXP3 Transcription buffer set (ThermoFisher), according to manufacturer's instruction. Fixation permeabilization and intracellular FOXP3 staining was performed for 30 minutes. For analysis of granzyme B, TNF $\alpha$  and IFN $\gamma$ , single cell suspensions were incubated in cIMDM (IMDM containing 8% FCS, 100 IU/ml penicillin, 100  $\mu\text{g}/\text{ml}$  streptomycin, 0.5%  $\beta$ -mercapto-ethanol), 50 ng/ml PMA, 1  $\mu\text{M}$  ionomycin and Golgi-Plug (1:1000; BD Biosciences) for 3 h at 37  $^{\circ}\text{C}$  prior to surface staining. For analysis of  $T_{\text{reg}}$  proliferation *in vivo*, mice were injected with the thymidine analog EdU (200  $\mu\text{g}$ ) 24 and 48h prior to sacrifice. DNA incorporation of EdU was measured using Click-iT<sup>TM</sup> EdU Cell Proliferation Kit for Imaging according to manufacturer's instruction. Cell suspensions were analyzed on a BD LSR2 SORP or BD Symphony SORP, or sorted on a FACS ARIA II (4 lasers), or FACS FUSION (5 lasers). Single cell suspensions for cell sorting were prepared under sterile conditions. Gating strategies for  $T_{\text{reg}}$  sorting as previously described<sup>63</sup>. See Key Resources Table for antibodies used. Absolute cell counts were determined using 123count eBeads (ThermoFisher) according to manufacturer's instruction.

### $T_{\text{reg}}$ suppression assays

$T_{\text{reg}}$ -T cell suppression assays were performed as previously described<sup>63</sup>. Briefly,  $T_{\text{regs}}$  (Live, CD45<sup>+</sup>, CD3<sup>+</sup>, CD8<sup>-</sup>, CD4<sup>+</sup>, CD25<sup>high</sup>) sorted from freshly isolated samples were activated overnight in IMDM containing 8% FCS, 100 IU/ml penicillin, 100  $\mu\text{g}/\text{ml}$  streptomycin, 0.5%  $\beta$ -mercapto-ethanol, 300U/mL IL-2, 1:5 bead:cell ratio CD3/CD28 coated beads (ThermoFisher). Per condition,  $5.0 \times 10^5$  cells were seeded in 96-wells plate, which were further diluted to appropriate ratios (1:1 – 1:8). Responder cells (Live, CD45<sup>+</sup>, CD3<sup>+</sup>, CD4<sup>+</sup>, CD25<sup>-</sup> and Live, CD45<sup>+</sup>, CD3<sup>+</sup>, CD8<sup>+</sup>) were rested overnight. Next, responder cells were

labelled with CellTraceViolet, and co-cultured with T<sub>regs</sub> in cIMDM supplemented with CD3/CD28 beads (1:5 bead cell ratio) for 96 h (without exogenous IL-2).

### **NK cell degranulation assay**

Single cell suspensions of murine LN and lung samples were plated in a 96-wells plate, and incubated in IMDM containing 8% FCS, 100 IU/ml penicillin, 100 µg/ml streptomycin, 0.5% β-mercapto-ethanol, Golgi-Plug and Golgi-Stop (1:1,000; BD Biosciences) and anti-CD107a (clone LAMP-1, 1:200, Biolegend) for 4 h at 37 °C. For stimulation, cells were additionally supplemented with 50 ng ml<sup>-1</sup> PMA, 1 mM ionomycin.

### **T<sub>reg</sub> - KEP serum co-culture assay**

5.0\*10<sup>4</sup> splenic KEP T<sub>regs</sub> sorted from freshly isolated samples were incubated for 96 h in 96-wells plated coated with 5 µg/mL anti-CD3 in IMDM containing 100 IU/ml penicillin, 100 µg/ml streptomycin, 0.5% β-mercapto-ethanol supplemented with 20% serum obtained from end-stage tumor-bearing KEP mice, or naïve littermates. Next, absolute cell counts were determined by flow cytometry as described above.

### **IL-33 protein analysis**

To quantify IL-33 protein in different tissues of KEP mice and littermates, LegendPlex BioAssay (BioLegend) was used according to manufacturers' instruction. Protein lysates from snap frozen tissue were prepared by pulverizing small tissue fragments (1-2mm<sup>2</sup>), which were incubated in RIPA buffer (50 mM Tris-HCl, pH 7.4, 150 mM NaCl, 1% NP40, 0.5% DOC, 0.1% SDS, 2 mM EDTA) complemented with protease and phosphatase inhibitors (Roche) for 30 minutes at 4 °C. Protein concentration was quantified using the BCA protein assay kit (Pierce). Samples were diluted to 4 mg/mL protein of which 40µL was used as input for IL-33 LegendPlex Bioassay according to manufacturers' instruction. Protein content (pg/mL) was determined using BioLegend LegendPlex analysis software.

### **Immunohistochemistry**

Immunohistochemical analyses were performed by the Animal Pathology facility at the Netherlands Cancer Institute. Formalin-fixed tissues were processed, sectioned and stained as described<sup>25</sup>. In brief, tissues were fixed for 24 h in 10% neutral buffered formalin, embedded in paraffin, sectioned at 4 µm and stained with haematoxylin and eosin (H&E) for histopathological evaluation. H&E slides were digitally processed using the Aperio ScanScope (Aperio). For immunohistochemical analysis, 5 µm paraffin sections were cut, deparaffinized and stained. To score pulmonary metastasis, lung sections were stained for cytokeratin-8 and metastatic nodules were counted by two independent researchers. To score axillary LN metastasis incidence, draining axillary (proper and accessory) LN of mice that did not develop macroscopic LN metastasis were stained for cytokeratin-8. Presence of cytokeratin-8<sup>+</sup> cells (≥1) within LNs was indicative of micro metastatic disease. Stained

tissue slides were digitally processed using the Aperio ScanScope. Brightness and contrast for representative images were adjusted equally among groups.

### **RNAseq sample preparation: T<sub>regs</sub>**

For transcriptome analysis of T<sub>regs</sub> from end-stage (225mm<sup>2</sup>) tumor-bearing KEP mice and WT controls, single cell suspensions were prepared from spleens, mammary LNs, lungs, blood, tumor and naïve WT mammary glands as described above. A minimum of 70,000 T<sub>regs</sub> (Live, CD45<sup>+</sup>, CD3<sup>+</sup>, CD4<sup>+</sup>, CD25<sup>high</sup>) were sorted in RLT buffer with 1% β-mercapto ethanol. Due to low abundance of T<sub>regs</sub> in WT mice, tissue of 3 mice was pooled for each WT T<sub>reg</sub> sample prior to sorting. Library preparation was performed as previously described<sup>64</sup>.

### **RNAseq sample preparation: NK cells**

For transcriptome analysis of NK cells of DT/PBS treated tumor-bearing (100mm<sup>2</sup>) *Foxp3*<sup>GFP-DTR</sup> mice, single cells suspensions were prepared from axillary LNs and lungs, as described above. A minimum of 5000 NK cells (Live, CD45<sup>+</sup>, CD3<sup>-</sup>, NKp46<sup>+</sup>, DX5<sup>+</sup>) were sorted in RLT buffer with 1% β-mercapto-ethanol. Library preparation was performed as previously described<sup>65</sup>, using 2100 Bioanalyzer System for library quality control.

### **RNAseq of T<sub>reg</sub> and NK cells**

Sorted T<sub>reg</sub> and NK cells were resuspended in RLT buffer + 1% β-mercapto-ethanol. Total RNA was extracted using RNeasy mini kit (Qiagen). RNA quality and quantity control was performed using Agilent RNA 6000 Pico Kit and 2100 Bioanalyzer System. RNA samples with an RNA Integrity Number > 8 were subjected to library preparation. The strand-specific reads (65bp single-end) were sequenced with the HiSeq 2500 machine. Demultiplexing of the reads was performed with Illumina's bcl2fastq. For T<sub>reg</sub> RNAseq, demultiplexed reads were aligned against the mouse reference genome (build 38) using TopHat (version 2.1.0, bowtie 1.1). TopHat was supplied with a known set of gene models (Ensembl version 77) and was guided to use the first-strand as the library-type. As additional parameters --pre-filter-multihits and --no-coverage were used. For NK cell RNAseq, demultiplexed reads were aligned against the mouse reference genome (build 38) using Hisat2. Hisat2 was supplied with a known set of gene models (Ensembl version 87).

### **RNAseq analysis**

In order to count the number of reads per gene, a custom script, itreecount (<https://github.com/NKI-GCF/itreecount>), has been used. This script is based on the same concept as HTSeq-count. A list of the total number of uniquely mapped sequencing reads for each gene that is present in the provided Gene Transfer Format (GTF) file was generated. For T<sub>reg</sub> RNAseq, differential expression was performed using the R package Limma/Voom on normalized counts. Resulting p-values are corrected for multiple testing. A gene was considered differentially expressed if the p-value < 0.05, and read counts > 30 in all samples of a group.

For PCA the genes that have no expression across all samples within the dataset were removed. Furthermore, the analysis was restricted to only those genes that have at least two counts per million (CPM) value, calculated via edgeR package (3.30.3) using 'cpm' function in all samples from the included conditions and in this way lowly abundant genes were excluded. PCA was performed using the 'prcomp' function on variance stabilizing transformed data with the 'vst' function from the DESeq2 package with default arguments and plotted by using ggplot2 package (3.3.3) in R language (version 4.0.2).

Hierarchical cluster analysis for the samples was performed using 'hclust' function with default arguments. Dendrogram was made by using 'dendro\_data' function from ggdendro package (0.1.22). Sample to sample distances obtained using 'dist' function on variance stabilizing transformed data were subjected to hierarchical cluster analysis and dendrogram preparation. Normalized counts from DESeqDataSet from the DESeq2 package were subjected to calculate correlation among the samples by using 'cor' function using spearman method in R language (version 4.0.2).

Differential gene expression analysis of NK cells was performed in R language (version 4.0.2) only on relevant samples using edgeR package (3.30.3) and default arguments with the design set either to PBS or DT-treatment group. Lowly abundant genes (< 2 CPM) from all the samples in a specific contrast were excluded. Furthermore, to avoid any biasness due to the variation among the replicates within a group, the analysis was confined to the genes which have read counts (> 2 CPM) among all the replicates from either of the two groups in a specific contrast. Genes were considered to be differentially expressed when the False discovery rate (FDR) was below 0.1 after the Benjamini–Hochberg multiple testing correction. MA plots were generated after differential expression analysis in R language (version 4.0.2).

### IPA and GSEA analysis

Pathway enrichment analysis of KEP/WT T<sub>regs</sub> RNAseq data was performed using Ingenuity Pathway Analysis software (QIAGEN), analyzing differentially expressed genes with q value < 0.05 for KEP/WT T<sub>regs</sub>. Gene Set Enrichment Analysis (GSEA)<sup>66</sup> was performed using GSEA software (v. 4.0.3) on RNAseq data (transcripts for which read count > 30 included) of KEP/WT T<sub>reg</sub> of indicated tissues, on gene sets obtained from<sup>26</sup>, and mSigDB Hallmark gene sets<sup>38</sup>. Permutations for each gene set was conducted 1000 times to obtain an empirical null distribution.

### Human sentinel LN sampling

Viable cells were collected from SLN from ten female patients diagnosed with clinically node negative BrC scheduled to undergo a SLN procedure between February and July 2014, as previously described<sup>14</sup>. None of the patients received neoadjuvant chemo- or hormone

therapy prior to the SLN procedure. These ten patients were part of a previously described larger cohort<sup>14</sup>, and were selected based on availability of (previously unpublished) NK cell flow cytometry data. Axillary healthy LN were retrieved after written informed consent from prophylactic mastectomy specimens (n=16) in the Antoni van Leeuwenhoek Hospital between 2012-2014. The collection of these samples was also previously described and approved by the local IRB<sup>14</sup>.

### Preparation of human LN samples

Viable cells were scraped from the cutting surface of a bisected SLN before routine histopathological examination and after confirmation by the pathologist that the SLN was suitable for cell harvesting (i.e. >0.5cm), as described<sup>14,67</sup>. SLN cells were subsequently washed twice in IMDM supplemented with 10% FCS, 100 I.E./ml sodium penicillin, 100 µg/ml streptomycin sulfate, 2 mM L-glutamine (P/S/G), and 0.01 mM β-mercapto-ethanol, counted, and used for immune phenotyping. FACS staining for surface and intracellular proteins was performed as described<sup>14</sup> and data were acquired on a FACSCalibur flow cytometer (Becton Dickinson). NK cell and T<sub>reg</sub> frequencies were determined using FlowJo software (version 10.7). See Key Resources Table for antibodies used.

### Statistical analysis

Data analyses were performed using GraphPad Prism (version 8). Data show means ± SEM unless stated otherwise. The statistical tests used are described in figure legends. For comparison of two groups of continuous data, Student's T-test and Mann Whitney's T Test were used as indicated. For comparison of a single variable between multiple groups of normally distributed continuous data, we used one-way ANOVA, followed by indicated post-hoc analyses. For comparison of ≥2 variables between multiple groups, two-way ANOVA was used, with Sidak's post-hoc analysis. Fisher's exact test was used to assess significant differences between categorical variables obtained from lymph node metastasis incidence experiments. All tests were performed two-tailed. P-values < 0.05 were considered statistically significant. Sample sizes for mouse intervention experiments were predetermined using G\*Power software (version 3.1). *In vivo* interventions and RNAseq experiments were performed once with indicated sample sizes, unless otherwise indicated. In vitro experiments were repeated independently as indicated, with at least three biological replicates per condition. Asterisks indicate statistically significant differences compared to WT. \* P < 0.05, \*\* P < 0.01, \*\*\* P < 0.001, \*\*\*\* P < 0.0001.



## REFERENCES

1. DeSantis, C. E. *et al.* Breast cancer statistics, 2019. *CA. Cancer J. Clin.* **69**, 438–451 (2019).
2. Lambert, A. W., Pattabiraman, D. R. & Weinberg, R. A. Emerging Biological Principles of Metastasis. *Cell* **168**, 670–691 (2017).
3. Garner, H. & de Visser, K. E. Immune crosstalk in cancer progression and metastatic spread: a complex conversation. *Nat. Rev. Immunol.* 1–15 (2020) doi:10.1038/s41577-019-0271-z.
4. Angelova, M. *et al.* Evolution of Metastases in Space and Time under Immune Selection. *Cell* **175**, 751–765.e16 (2018).
5. Plitas, G. & Rudensky, A. Y. Regulatory T Cells in Cancer. *Annu. Rev. Cancer Biol.* **4**, 459–477 (2020).
6. Plitas, G. *et al.* Regulatory T Cells Exhibit Distinct Features in Human Breast Cancer. *Immunity* **45**, 1122–1134 (2016).
7. Kos, K. & de Visser, K. E. The Multifaceted Role of Regulatory T Cells in Breast Cancer. *Annu. Rev. Cancer Biol.* **5**, (2021).
8. Liu, S. *et al.* Prognostic significance of FOXP3+ tumor-infiltrating lymphocytes in breast cancer depends on estrogen receptor and human epidermal growth factor receptor-2 expression status and concurrent cytotoxic T-cell infiltration. *Breast Cancer Res.* **16**, (2014).
9. Decker, T. *et al.* Increased number of regulatory T cells (T-regs) in the peripheral blood of patients with Her-2/neu-positive early breast cancer. *J. Cancer Res. Clin. Oncol.* **138**, 1945–1950 (2012).
10. Liyanage, U. K. *et al.* Prevalence of Regulatory T Cells Is Increased in Peripheral Blood and Tumor Microenvironment of Patients with Pancreas or Breast Adenocarcinoma. *J. Immunol.* **169**, 2756–2761 (2002).
11. Perez, S. A. *et al.* CD4+CD25+ Regulatory T-Cell Frequency in HER-2/neu (HER)-Positive and HER-Negative Advanced-Stage Breast Cancer Patients. *Clin. Cancer Res.* **13**, 2714–2721 (2007).
12. Wolf, A. M. *et al.* Increase of Regulatory T Cells in the Peripheral Blood of Cancer Patients. *Clin. Cancer Res.* **9**, 606–612 (2003).
13. Wang, L. *et al.* Connecting blood and intratumoral Treg cell activity in predicting future relapse in breast cancer. *Nat. Immunol.* **20**, 1220–1230 (2019).
14. van Pul, K. M. *et al.* Selectively hampered activation of lymph node-resident dendritic cells precedes profound T cell suppression and metastatic spread in the breast cancer sentinel lymph node. *J. Immunother. Cancer* **7**, 133 (2019).
15. Faghiih, Z. *et al.* Immune profiles of CD4+ lymphocyte subsets in breast cancer tumor draining lymph nodes. *Immunol. Lett.* **158**, 57–65 (2014).
16. Mansfield, A. S. *et al.* Simultaneous Foxp3 and IDO expression is associated with sentinel lymph node metastases in breast cancer. *BMC Cancer* **9**, (2009).
17. Núñez, N. G. *et al.* Tumor invasion in draining lymph nodes is associated with Treg accumulation in breast cancer patients. *Nat. Commun.* **11**, 1–15 (2020).
18. Jiang, D., Gao, Z., Cai, Z., Wang, M. & He, J. Clinicopathological and prognostic significance of FOXP3+ tumor infiltrating lymphocytes in patients with breast cancer: A meta-analysis. *BMC Cancer* **15**, (2015).
19. Clark, N. M. *et al.* Regulatory T Cells Support Breast Cancer Progression by Opposing IFN- $\gamma$ -Dependent Functional Reprogramming of Myeloid Cells. *Cell Rep.* **33**, 108482 (2020).
20. Gómez-Cuadrado, L., Tracey, N., Ma, R., Qian, B. & Brunton, V. G. Mouse models of metastasis: progress and prospects. *Dis. Model. Mech.* **10**, 1061–1074 (2017).
21. Bos, P. D., Plitas, G., Rudra, D., Lee, S. Y. & Rudensky, A. Y. Transient regulatory T cell ablation deters oncogene-driven breast cancer and enhances radiotherapy. *J. Exp. Med.* **210**, 2435–2466 (2013).
22. Liu, J. *et al.* Improved efficacy of neoadjuvant compared to adjuvant immunotherapy to eradicate metastatic disease. *Cancer Discov.* **6**, 1382–1399 (2016).
23. Hughes, E. *et al.* Primary breast tumours but not lung metastases induce protective anti-tumour immune responses after Treg-depletion. *Cancer Immunol. Immunother.* 1–11 (2020) doi:10.1007/s00262-020-02603-x.
24. Derksen, P. W. B. *et al.* Somatic inactivation of E-cadherin and p53 in mice leads to metastatic lobular mammary carcinoma through induction of anoikis resistance and angiogenesis. *Cancer Cell* **10**, 437–449 (2006).
25. Doornebal, C. W. *et al.* A Preclinical Mouse Model of Invasive Lobular Breast Cancer Metastasis. *Cancer Res.* **73**, 353 LP – 363 (2013).
26. Magnuson, A. M. *et al.* Identification and validation of a tumor-infiltrating Treg transcriptional signature conserved across species and tumor types. *PNAS* **115**, E10672–E10681 (2018).
27. Cao, X. *et al.* Granzyme B and Perforin Are Important for Regulatory T Cell-Mediated Suppression of Tumor Clearance. *Immunity* **27**, 635–646 (2007).
28. Pastille, E. *et al.* The IL-33/ST2 pathway shapes the regulatory T cell phenotype to promote intestinal cancer. *Mucosal Immunol.* **12**, 990–1003 (2019).

29. Li, A. *et al.* IL-33 Signaling Alters Regulatory T Cell Diversity in Support of Tumor Development. *Cell Rep.* **29**, 2998-3008.e8 (2019).
30. Son, J. *et al.* Tumor-Infiltrating Regulatory T Cell Accumulation in the Tumor Microenvironment is Mediated by IL33/ST2 Signaling. *Cancer Immunol. Res.* **8**, canimm.0828.2019 (2020).
31. Matta, B. M. & Turnquist, H. R. Expansion of regulatory T cells in vitro and in vivo by IL-33. in *Methods in Molecular Biology* vol. 1371 29–41 (Humana Press Inc., 2016).
32. Holgado, A. *et al.* IL-33trap is a novel IL-33–neutralizing biologic that inhibits allergic airway inflammation. *J. Allergy Clin. Immunol.* **144**, 204–215 (2019).
33. Sun, L. *et al.* Divenn: An interactive and integrated web-based visualization tool for comparing gene lists. *Front. Genet.* **10**, 421 (2019).
34. Coffelt, S. B. *et al.* IL-17-producing  $\gamma\delta$  T cells and neutrophils conspire to promote breast cancer metastasis. *Nature* **522**, 345–348 (2015).
35. Arce Vargas, F. *et al.* Fc-Optimized Anti-CD25 Depletes Tumor-Infiltrating Regulatory T Cells and Synergizes with PD-1 Blockade to Eradicate Established Tumors. *Immunity* **46**, 577–586 (2017).
36. Paul, S. & Lal, G. The Molecular Mechanism of Natural Killer Cells Function and Its Importance in Cancer Immunotherapy. *Front. Immunol.* **0**, 1124 (2017).
37. Duhon, V. *et al.* NK cell–intrinsic Fc $\epsilon$ R1y limits CD8+ T-cell expansion and thereby turns an acute into a chronic viral infection. *PLoS Pathog.* **15**, e1007797 (2019).
38. Liberzon, A. *et al.* The Molecular Signatures Database Hallmark Gene Set Collection. *Cell Syst.* **1**, 417–425 (2015).
39. Chiossone, L. *et al.* Maturation of mouse NK cells is a 4-stage developmental program. *Blood* **113**, 5488–5496 (2009).
40. Hayakawa, Y. & Smyth, M. J. CD27 Dissects Mature NK Cells into Two Subsets with Distinct Responsiveness and Migratory Capacity. *J. Immunol.* **176**, 1517–1524 (2006).
41. Poli, A. *et al.* CD56bright natural killer (NK) cells: An important NK cell subset. *Immunology* vol. 126 458–465 (2009).
42. Kim, S. T. *et al.* Tumor-infiltrating lymphocytes, tumor characteristics, and recurrence in patients with early breast cancer. *Am. J. Clin. Oncol. Cancer Clin. Trials* **36**, 224–231 (2013).
43. Dings, P. J. M., Elferink, M. A. G., Strobbe, L. J. A. & de Wilt, J. H. W. The Prognostic Value of Lymph Node Ratio in Node-Positive Breast Cancer: A Dutch Nationwide Population-Based Study. *Ann. Surg. Oncol.* **20**, 2607–2614 (2013).
44. Beenken, S. W. *et al.* Axillary Lymph Node Status, But Not Tumor Size, Predicts Locoregional Recurrence and Overall Survival After Mastectomy for Breast Cancer. *Ann. Surg.* **237**, 732–739 (2003).
45. López-Soto, A., Gonzalez, S., Smyth, M. J. & Galluzzi, L. Control of Metastasis by NK Cells. *Cancer Cell* vol. 32 135–154 (2017).
46. Huntington, N. D., Cursons, J. & Rautela, J. The cancer–natural killer cell immunity cycle. *Nature Reviews Cancer* vol. 20 437–454 (2020).
47. Ghiringhelli, F. *et al.* CD4+CD25+ regulatory T cells inhibit natural killer cell functions in a transforming growth factor- $\beta$ -dependent manner. *J. Exp. Med.* **202**, 1075–1085 (2005).
48. Mamessier, E. *et al.* Human breast cancer cells enhance self tolerance by promoting evasion from NK cell antitumor immunity. *J. Clin. Invest.* **121**, 3609–3622 (2011).
49. Kim, R. *et al.* A potential role for peripheral natural killer cell activity induced by preoperative chemotherapy in breast cancer patients. *Cancer Immunol. Immunother.* **68**, 577–585 (2019).
50. Wing, K. *et al.* CTLA-4 control over Foxp3+ regulatory T cell function. *Science (80- )*. **322**, 271–275 (2008).
51. Schuijs, M. J. *et al.* ILC2-driven innate immune checkpoint mechanism antagonizes NK cell antimetastatic function in the lung. *Nat. Immunol.* **21**, 998–1009 (2020).
52. Reiter, J. G. *et al.* Lymph node metastases develop through a wider evolutionary bottleneck than distant metastases. *Nat. Genet.* **52**, 692–700 (2020).
53. Zhong, W. *et al.* Comparison of the molecular and cellular phenotypes of common mouse syngeneic models with human tumors. *BMC Genomics* **21**, 2 (2020).
54. Gutierrez, W. R. *et al.* Divergent immune landscapes of primary and syngeneic Kras-driven mouse tumor models. *Sci. Rep.* **11**, 1098 (2021).
55. Hemmers, S., Schizas, M. & Rudensky, A. Y. T reg cell-intrinsic requirements for ST2 signaling in health and neuroinflammation. *J. Exp. Med.* **218**, (2021).
56. Sun, Z. *et al.* A next-generation tumor-targeting IL-2 preferentially promotes tumor-infiltrating CD8+ T-cell response and effective tumor control. *Nat. Commun.* **10**, (2019).
57. Wellenstein, M. D. *et al.* Loss of p53 triggers WNT-dependent systemic inflammation to drive breast cancer metastasis. *Nature* **572**, 538–542 (2019).
58. Annunziato, S. *et al.* Modeling invasive lobular breast carcinoma by CRISPR / Cas9-mediated somatic genome editing of the mammary gland. *Genes Dev.* **30**, 1470–1480 (2016).

59. Annunziato, S. *et al.* Comparative oncogenomics identifies combinations of driver genes and drug targets in BRCA1-mutated breast cancer. *Nat. Commun.* **10**, (2019).
60. Boelens, M. C. *et al.* PTEN Loss in E-Cadherin-Deficient Mouse Mammary Epithelial Cells Rescues Apoptosis and Results in Development of Classical Invasive Lobular Carcinoma. *Cell Rep.* **16**, 2087–2101 (2016).
61. Kim, J. M., Rasmussen, J. P. & Rudensky, A. Y. Regulatory T cells prevent catastrophic autoimmunity throughout the lifespan of mice. *Nat. Immunol.* **8**, 191–7 (2007).
62. Huijbers, I. J. *et al.* Using the GEMM-ESC strategy to study gene function in mouse models. *Nat. Protoc.* **10**, 1755–1785 (2015).
63. Kos, K., van Baalen, M., Meijer, D. A. & de Visser, K. E. Flow cytometry-based isolation of tumor-associated regulatory T cells and assessment of their suppressive potential. in *Methods in Enzymology* (2019). doi:10.1016/bs.mie.2019.07.035.
64. Aslam, M. A. *et al.* The Ig heavy chain protein but not its message controls early B cell development. *Proc. Natl. Acad. Sci. U. S. A.* **117**, 31343–31352 (2020).
65. Picelli, S. *et al.* Full-length RNA-seq from single cells using Smart-seq2. *Nat. Protoc.* **9**, 171–181 (2014).
66. Subramanian, A. *et al.* Gene set enrichment analysis: A knowledge-based approach for interpreting genome-wide expression profiles. *Proc. Natl. Acad. Sci. U. S. A.* **102**, 15545–15550 (2005).
67. Vuytsteke, R. J. C. L. M. *et al.* Sampling tumor-draining lymph nodes for phenotypic and functional analysis of dendritic cells and T cells. *Am. J. Pathol.* **161**, 19–26 (2002).

## SUPPLEMENTARY MATERIALS

Data file S1: Differentially expressed genes KEP/WT T<sub>regs</sub> for indicated tissues, and distribution across tissue. Related to Figure 2 and 3.

Data file S2: Differentially expressed genes of DT/PBS treated NK cells for indicated tissues, and distribution across tissue. Related to Figure 5. These files are available in the online version of the paper.



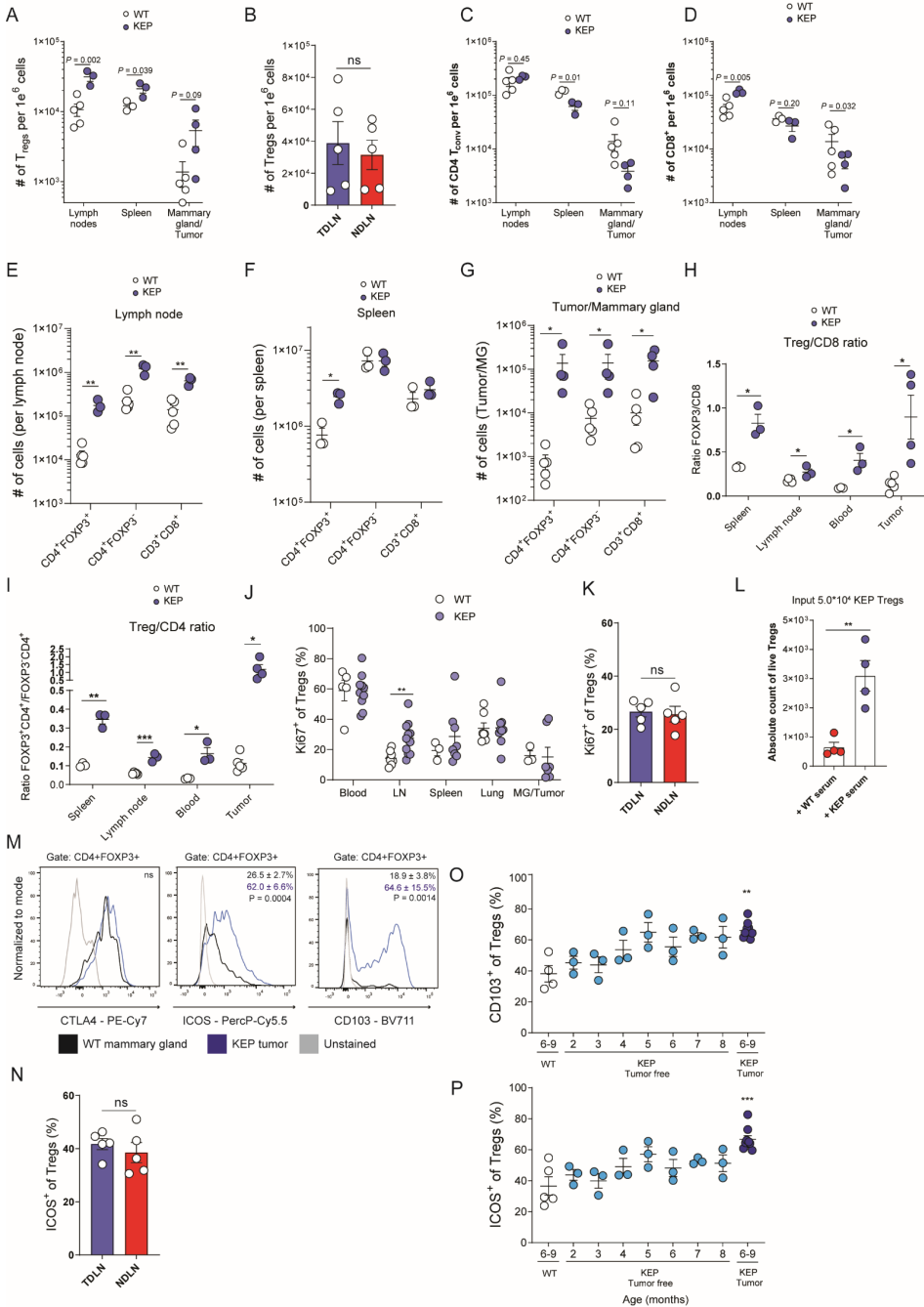


**FIGURE S1. T<sub>regs</sub> selectively expand in mammary tumor-bearing mice. Related to figure 1.**

**A-D.** Absolute cell counts of T<sub>regs</sub> (**A,B**), T<sub>conv</sub> (**C**) and CD8<sup>+</sup> T cells (**D**) per 1e<sup>6</sup> cells in indicated tissues (n=3 mice/group) of tumor-bearing (225mm<sup>2</sup>) KEP mice and WT controls (n=3-5 mice/group). **E-G.** Total absolute cell counts of indicated T cell population per lymph node (**E**), spleen (**F**) and tumor/mammary gland (**G**) of tumor-bearing (225mm<sup>2</sup>) KEP mice and WT controls (n=3-5 mice/group). **H-I.** Ratio (based on data in **A,C,D**) of FOXP3<sup>+</sup>CD4<sup>+</sup>/CD8<sup>+</sup> T cells (**H**) and FOXP3<sup>+</sup>CD4<sup>+</sup>/FOXP3<sup>+</sup>CD4<sup>+</sup> (**I**) in indicates tissue of tumor-bearing (225mm<sup>2</sup>) KEP mice and WT controls. **J.** Quantification of Ki67 expression on T<sub>regs</sub> in tumor-bearing KEP mice (100-225mm<sup>2</sup>) and WT controls in indicated tissues as determined by flow cytometry (n=3-10 mice/group). **K.** Quantification of Ki67 expression on T<sub>regs</sub> in TDLN and NDLN of tumor-bearing KEP mice (225mm<sup>2</sup>) by flow cytometry (n=5 mice/group). **L.** 5\*10<sup>4</sup> KEP T<sub>regs</sub> (CD4<sup>+</sup>CD25<sup>+</sup>) were cultured for 96 hours with 5 µg/mL anti-CD3 and 20% serum obtained from WT controls or tumor-bearing KEP mice (225mm<sup>2</sup>). Quantification of live KEP T<sub>regs</sub> is shown (data pooled from 2 independent experiment with 2 biological replicates per experiment). **M.** Representative histograms depicting expression of intracellular CTLA4, ICOS and CD103 gated on CD4<sup>+</sup> FOXP3<sup>+</sup> T cells, in (225m<sup>2</sup>) tumors of KEP (blue) mice versus WT controls (black) by flow cytometry. % represent mean frequency (n=3-7 mice/group). **N.** Quantification of ICOS expression on T<sub>regs</sub> in TDLN and NDLN of tumor-bearing KEP mice (225mm<sup>2</sup>) by flow cytometry (n=5 mice/group). **O-P.** Frequencies of CD103<sup>+</sup> cells (**O**) and ICOS (**P**) of FOXP3<sup>+</sup>CD4<sup>+</sup> T cells in blood of tumor-free, and tumor-bearing (225mm<sup>2</sup>) KEP mice and WT controls (n=3-10 mice/group). Data in A-L, N-P show mean ± S.E.M. P-values are determined by Unpaired Students T-test (A-F,K,M,N), Unpaired Students T-test with Holm-Sidak correction for multiple testing (H-I,J), Mann-Whitney Test (G,L) and Kruskal-Wallis test with Dunn's multiple comparison test (O,P).

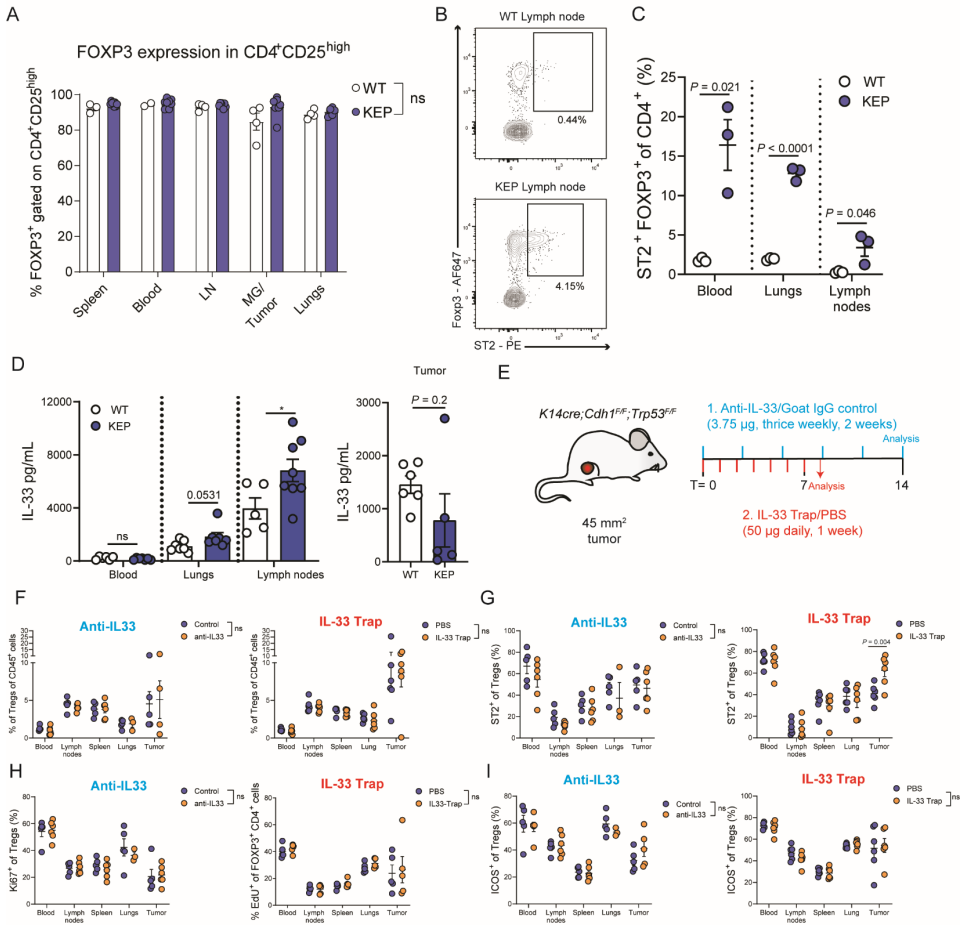




**FIGURE S2. Role of IL-33 for T<sub>regs</sub> in KEP tumor-bearing mice. Related to figure 2.**

**A.** Quantification of FOXP3 expression in CD4<sup>+</sup>CD25<sup>high</sup> T cells in indicated tissues of WT and tumor-bearing KEP mice (n=4-8 mice/group). **B.** Representative dot plot depicting ST2 expression on CD4<sup>+</sup> cells in TDLNs of 100mm<sup>2</sup> tumor-bearing KEP mice and WT controls. Gated on Live, CD45<sup>+</sup>, CD3<sup>+</sup>CD4<sup>+</sup> cells. **C.** Quantification of data shown in **(B)**, for indicated tissues (n=3 mice/group). **D.** Legendplex analysis of IL-33 protein content in serum, lung, LN and KEP tumor lysates. Tissue samples obtained from tumor-bearing (225mm<sup>2</sup>) KEP mice and WT controls (n=5-8 biological replicates per group). **E.** Schematic overview of IL-33 blockade strategies. Tumor-bearing KEP mice were treated with either anti-IL-33 (n=6 mice/group) /goat IgG control (n=5 mice/group) (3.75 µg, thrice weekly), or with IL-33Trap/PBS (n=6/group 50 µg/daily) for indicated timepoints starting at a tumor size of ~45mm<sup>2</sup>. IL-33Trap/PBS treated mice received 200 µg EdU 48h and 24h prior to sacrifice to analyse cell proliferation. **F-I** Analysis of % T<sub>regs</sub> of CD45<sup>+</sup> cells (**F**), ST2 expression on T<sub>regs</sub> (**G**), Ki67 expression on T<sub>regs</sub> (left panel), or EdU<sup>+</sup> T<sub>regs</sub> (right panel) (**H**), ICOS expression on T<sub>regs</sub> (**I**) in indicated tissue of mice receiving treatments as indicated in (n=3 for lungs anti-IL-33, n=5-6 for other comparison). Data in A, C-D, F-I show mean ± S.E.M. P-values are determined by Unpaired Students T-test (C-D). Unpaired Students T-test with Holm-Sidak correction for multiple testing (A), 2-way ANOVA with Holm-Sidak's multiple comparison test (F-I).

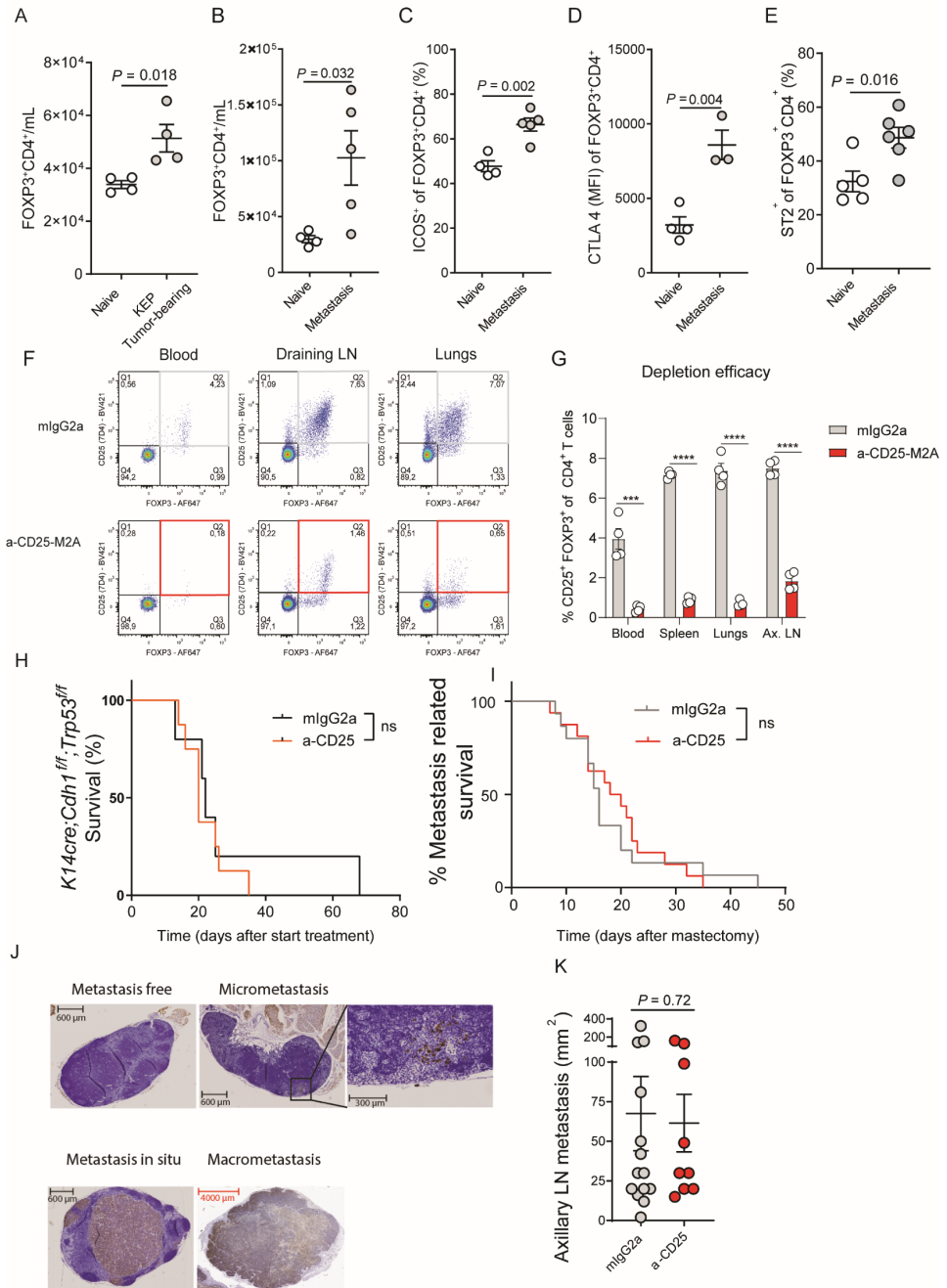


**FIGURE S3. Systemic T<sub>reg</sub> activation in mice bearing breast cancer metastasis. Related to figure 4.**

**A-B.** Absolute cell count of T<sub>reg</sub> (CD4<sup>+</sup>FOXP3<sup>+</sup> T cells) in blood of naïve mice, versus mice bearing orthotopically transplanted primary KEP tumors prior to mastectomy (80-100mm<sup>2</sup>) (**A**), or end-stage metastatic disease (**B**) (n=4-5 mice/group). **C-E.** Analysis of ICOS (**C**) and CTLA4 (**D**) and ST2 (**E**) expression on T<sub>regs</sub> in blood of mice with end-stage metastatic disease, versus naïve controls (n=4-6 mice/group). **F.** Representative dot plots of CD25 and FOXP3 expression, gated on live CD4<sup>+</sup> T cells in blood, draining axillary lymph node and lungs of KEP tumor-bearing mice treated with mlgG2a or anti-CD25. Mice were sacrificed 3 days after start treatment (n=4 mice/group). **G.** Quantification of CD25<sup>+</sup>FOXP3<sup>+</sup> of CD4<sup>+</sup> T cell gate (Q2) shown in (**F**) in indicated tissues of KEP tumor-bearing mice treated with mlgG2a or anti-CD25. Mice were sacrificed 3 days after start treatment (n=4 mice/group). **H.** Kaplan-Meier plot of tumor-specific survival of KEP mice treated with mlgG2a or anti-CD25. Treatment (weekly injection of 200 µg antibody) was initiated at tumor size of 25mm<sup>2</sup>, and continued until end-stage (225mm<sup>2</sup>) (n=5-7 mice/group). **I.** Metastasis related survival after mastectomy of KEP tumor-bearing mice receiving weekly neoadjuvant treatment of 200 µg mlgG2a or anti-CD25. **J.** Representative immunohistochemical keratin 8 staining depicting axillary TDLNs in mice with end-stage metastatic disease with, and without metastatic infiltration of keratin 8<sup>+</sup> cancer cells. **K.** LN tumor size (mm<sup>2</sup>) upon sacrifice in mice with LN metastasis, treated with mlgG2a or anti-CD25-M2a (n=9-14 mice/group). Data in A-E, G, K show mean ± S.E.M. P-value was determined by Mann Whitney test (A-E, K), Unpaired Students T-test with Holm-Sidak correction for multiple testing (G) log-rank test (H,I).

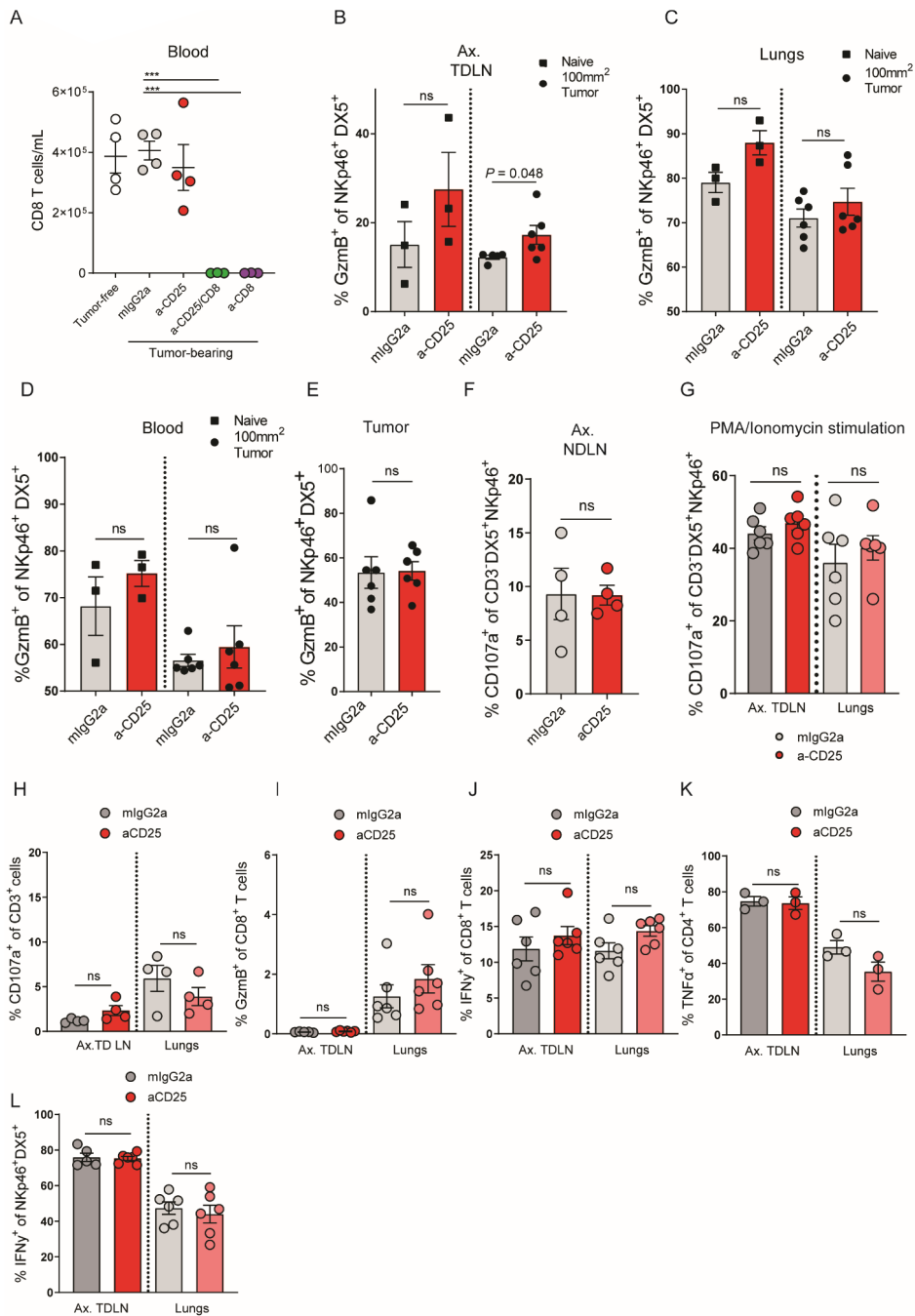
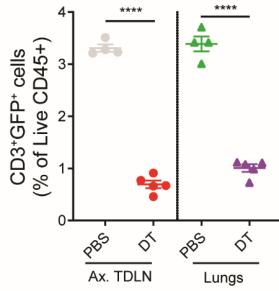


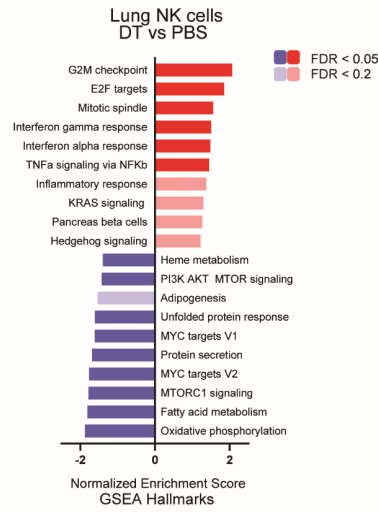
**FIGURE S4. Tissue-specific impact of T<sub>reg</sub> depletion on T- and NK cell activation. Related to figure 5.**

**A.** Absolute count of CD8<sup>+</sup> T cells/mL of blood in tumor-free and mice bearing orthotopically transplanted KEP tumors treated with indicated treatments, 8-10 days after start of treatment (n=3-4 mice/group). **B-E.** Granzyme B expression 3h after *ex vivo* stimulation of NKp46<sup>+</sup>DX5<sup>+</sup> NK cells from axillary TDLNs (**B**), lungs (**C**), blood (**D**) tumor (**E**) of mice bearing orthotopically transplanted KEP tumors (100mm<sup>2</sup>) and WT controls (n=3/group), receiving weekly neoadjuvant treatment of 200 µg anti-CD25 or mlgG2a (n=6/group). **F.** *Ex vivo* CD107a expression of unstimulated NKp46<sup>+</sup>DX5<sup>+</sup>NK cells from contralateral Ax. NDLN of mice bearing orthotopically transplanted KEP tumors (100mm<sup>2</sup>) receiving weekly neoadjuvant treatment of 200 µg anti-CD25 or mlgG2a (n=6/group). **G.** CD107a expression 4h after *ex vivo* stimulation of NKp46<sup>+</sup>DX5<sup>+</sup>NK cells with PMA/ionomycin from Ax. TDLNs and lungs of mice bearing orthotopically transplanted KEP tumors (100mm<sup>2</sup>) receiving weekly neoadjuvant treatment of 200 µg anti-CD25 or mlgG2a (n=6/group). **H.** *Ex vivo* CD107a expression of unstimulated CD45<sup>+</sup>CD3<sup>+</sup> cells from Ax. TDLNs of mice bearing orthotopically transplanted KEP tumors (100mm<sup>2</sup>) receiving weekly neoadjuvant treatment of 200 µg anti-CD25 or mlgG2a (n=4/group). **I-L.** Expression of GzmB (**I**), and IFN $\gamma$  by CD8<sup>+</sup> T cells (**J**), TNF $\alpha$  by CD4<sup>+</sup> T cells (**K**), IFN $\gamma$  by NK cells (**L**) following a 3 hour *ex vivo* stimulation in Ax. TDLNs and lungs of mice bearing orthotopically transplanted KEP tumors (100mm<sup>2</sup>) Receiving weekly neoadjuvant treatment of 200 µg anti-CD25 or mlgG2a (n=3-6 mice/group). Data in A-L show mean  $\pm$  S.E.M. P-value was determined by Mann-Whitney test (B-L), One-way ANOVA (A). \*\*\* P < 0.001.

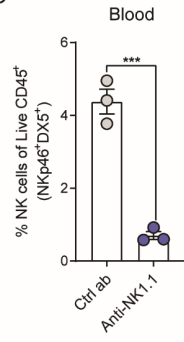
A



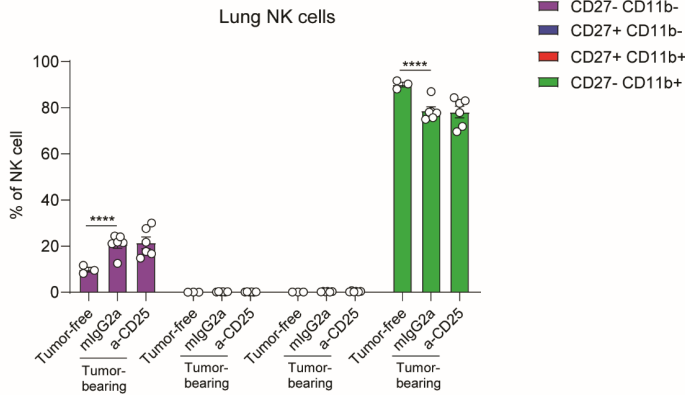
B



C



D



E

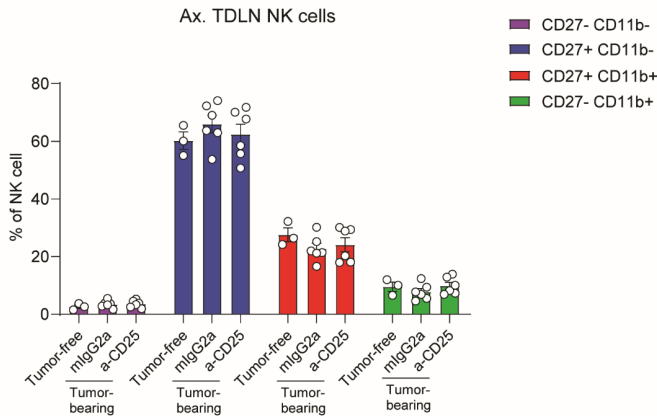


**FIGURE S5. Kinetics of NK cells in KEP tumor-bearing mice. Related to figure 5 and 6.**

**A.** Frequency of CD3<sup>+</sup>GFP<sup>+</sup> cells of total live CD45<sup>+</sup> cells in Ax. TDLNs and lungs of *Foxp3*<sup>GFP-DTR</sup> mice bearing orthotopically transplanted KEP tumors (100mm<sup>3</sup>), receiving weekly treatment of PBS or 25 µg DT (n=5/group). **B.** GSEA analysis of lung NK cells, DT vs PBS, using hallmark gene sets. Top 10 enriched up- and downregulated pathways are shown. **C.** Frequency of CD3<sup>+</sup>NKp46<sup>+</sup>DX5<sup>+</sup> NK cells of total live CD45<sup>+</sup> cells in blood of mice bearing orthotopically transplanted KEP tumors, 8-10 days after start of indicated treatment (n=3/group). **D-E.** Frequency of NK cells in different maturation states based on expression of CD27 and CD11b in lungs (**D**) and Ax. TDLNs (**E**) in tumor-free (n=3/group), or tumor-bearing mice treated with mIgG2a or anti-CD25 (n=6/group). Data in A,C-E show mean ± S.E.M. P-value was determined by Unpaired Student's T-test (A, C), Two-way ANOVA with Dunnett's correction for multiple testing (D-E). \*\*\* P < 0.001, \*\*\*\* P < 0.0001.